Title

Mechanical strain can increase segment number in live chick embryos

Author list

Ben K.A. Nelemans[1*], Manuel Schmitz[1*], Hannan Tahir[1,2], Roeland M.H. Merks[2,3], Theodoor H. Smit[4,5]

* These authors contributed equally to this work.

Corresponding author is Theodoor H. Smit (email: t.h.smit@amc.nl)

Affiliations

1 Department of Orthopaedic Surgery, VU University Medical Center, Amsterdam Movement Sciences, Amsterdam, The Netherlands

2 Centrum Wiskunde & Informatica, Amsterdam, The Netherlands.

3 Mathematical Institute, Leiden University, Leiden, The Netherlands

4 Department of Medical Biology, Academic Medical Center, Amsterdam, The Netherlands

5 Amsterdam Movement Sciences Research Institute, The Netherlands

Abstract

Physical cues, experienced during early embryonic development, can influence species-specific vertebral numbers. Here we show that mechanical stretching of live chicken embryos can induce the formation of additional somites and thereby modify early segmental patterning. Stretching deforms the somites, and results in a cellular reorganization that forms stable daughter somites. Cells from the somite core thereby undergo mesenchymal-to-epithelial transitions (MET), thus meeting the geometrical demand for more border cells. Using a Cellular Potts Model, we suggest that this MET occurs through lateral induction by the existing epithelial cells. Our results indicate that self-organizing properties of the somitic mesoderm generate phenotypic plasticity that allows it to cope with variations in the mechanical environment. This plasticity may provide a novel mechanism for explaining how vertebral numbers in species may have increased during evolution. Additionally, by preventing the formation of transitional vertebrae, these self-organization qualities of somites may be selectively advantageous.

Introduction

A segmented spine is the characteristic feature of the vertebrate body plan, which provides mechanical support, flexibility, and protection of the spinal cord. Vertebral numbers vary considerably among species, ranging from six in frogs to several hundred in snakes (Richardson, Allen, Wright, Raynaud, & Hanken, 1998). The evolvability of the vertebral column allows vertebrates to adapt to diverse habitats and acquire matching locomotor styles by tuning the number of body segments (Galis et al., 2014a).

Patterning of the vertebrate body originates early in embryogenesis when the paraxial mesoderm on both sides of the midline segments into somites, which contain the predecessor

cells of vertebrae, ribs, muscles and skin. Somites are cell blocks in which a core of mesenchymal cells, the somitocoel, is surrounded by an epithelial layer (Kulesa, Schnell, Rudloff, Baker, & Maini, 2007; Martins et al., 2009); they also impose a segmented organization on the peripheral nervous system. The sequential partitioning of the paraxial mesoderm appears to be imposed by a molecular clock and a travelling wave of maturation created by a system of signalling gradients (Hubaud & Pourquié, 2014). This complex signalling network appears well conserved throughout the vertebrate phylum. The variation in somite numbers (and vertebral numbers) between species is presumably caused by mutations that lead to changes in the speed of the clock period or the elongation rate of the mesoderm, which both affect segmentation rate and somite size (Gomez et al., 2008; Gomez & Pourquie, 2009; Herrgen et al., 2010).

Despite the intricately controlled network of the clock-and-wavefront mechanism, vertebral numbers in fish (Beacham & Murray, 1986; Hubbs, 1922; Tibblin, Berggren, Nordahl, Larsson, & Forsman, 2016), amphibians (Jockusch, 1997; Peabody & Brodie Jr., 1975), reptiles (Osgood, 1978), mammals (Lecyk, 1966) and birds (Lindsey & Moodie, 1967) may be influenced during early embryonic development by environmental cues such as temperature, salinity or light conditions. Mechanics may be another physical cue that induces different phenotypes of segmental patterning. In the framework of the Extended Evolutionary Synthesis, it has been argued according to the ‘side-effect hypothesis’, that morphological novelties in the body plan can result not only from genetic rearrangements, but also from mechanical cues exerted on self-organizing developing tissues (Laland et al., 2015; G. Müller, 1990; G. B. Müller, 2003). Somitic mesoderm possesses a certain capacity for self-organization, as somite-like structures can form ectopically in the absence of a clock or a wavefront (Dias, de Almeida, Belmonte, Glazier, & Stern, 2014). The size of epithelializing

somites strongly correlates with embryonic growth (Tam, 1981), and hampering axial elongation of the embryo leads to disorganized somites (Stern & Bellairs, 1984). Somite formation also requires the contraction of cells in the PSM (Duess, Fujiwara, Corcionivoschi, Puri, & Thompson, 2013) and mechanical adhesion to the surrounding fibronectin matrix (Hubaud, Regev, Mahadevan, & Pourquié, 2017; Martins et al., 2009).

On the basis of these observations, we hypothesized that if somitic mesoderm is self-organizing under the influence of biomechanical cues, mechanical stretching may then suffice to induce morphological changes in the segmented vertebrate body plan.

To test this hypothesis, we developed a novel experimental setup to apply controlled strains to live chicken embryos. Time-lapse imaging confirmed that, given sufficient strain, mesodermal patterning can indeed be modulated (Fig S1). This suggests that mechanical cues can affect morphogenesis and may be an explanatory factor for variation in vertebral numbers in the scope of the 'side-effect hypothesis'.

Results

To test the effect of mechanical stretching on somitogenesis, stage HH8-9 chick embryos (Hamburger & Hamilton, 1951) were cultured *ex ovo* in modified submerged filter paper sandwiches (Schmitz, Nelemans, & Smit, 2016) and stretched along their body axis twice for 51 to 54 minutes at 1.2 µm/s (Fig S1). As a result, the embryos experienced strain values of 23 ± 3% (average ± SD) after the first pull and 19 ± 3% after the second pull. Approximately 12 hours after manipulation, the mesodermal segmentation of one third (19/57) of all stretched embryos was clearly disturbed, unlike that of control embryos (Fig 1A and B). Time-lapse microscopic imaging (Schmitz et al., 2016) revealed that somites budded off from

93 the PSM at regular intervals of 79 ± 8 minutes in controls and 80 ± 6 minutes in stretched
94 samples. Stretched somites were more elongated than those in control embryos (Fig 1C-F,
95 Movie S1 and Movie S2). These deformed somites then regularly divided into what we call
96 “daughter somites”, and their morphology was consistent with somite divisions observed in
97 N-cadherin and Cadherin-11 knockout mice (Horikawa, Radice, Takeichi, & Chisaka, 1999;
98 Kimura et al., 1995). During daughter-somite formation, an invagination along the
99 mediolateral plane of the deformed somites appeared simultaneously to their separation from
100 the PSM (Fig 1F, Movie S2). It took several hours from the first appearance of this
101 mediolateral invagination for the somite to divide completely. Somite division in stretched
102 embryos appeared unilaterally or bilaterally, and often resulted in daughter somites of
103 different sizes (Movie S2, Fig S4, Fig S5 and Fig S8).
104

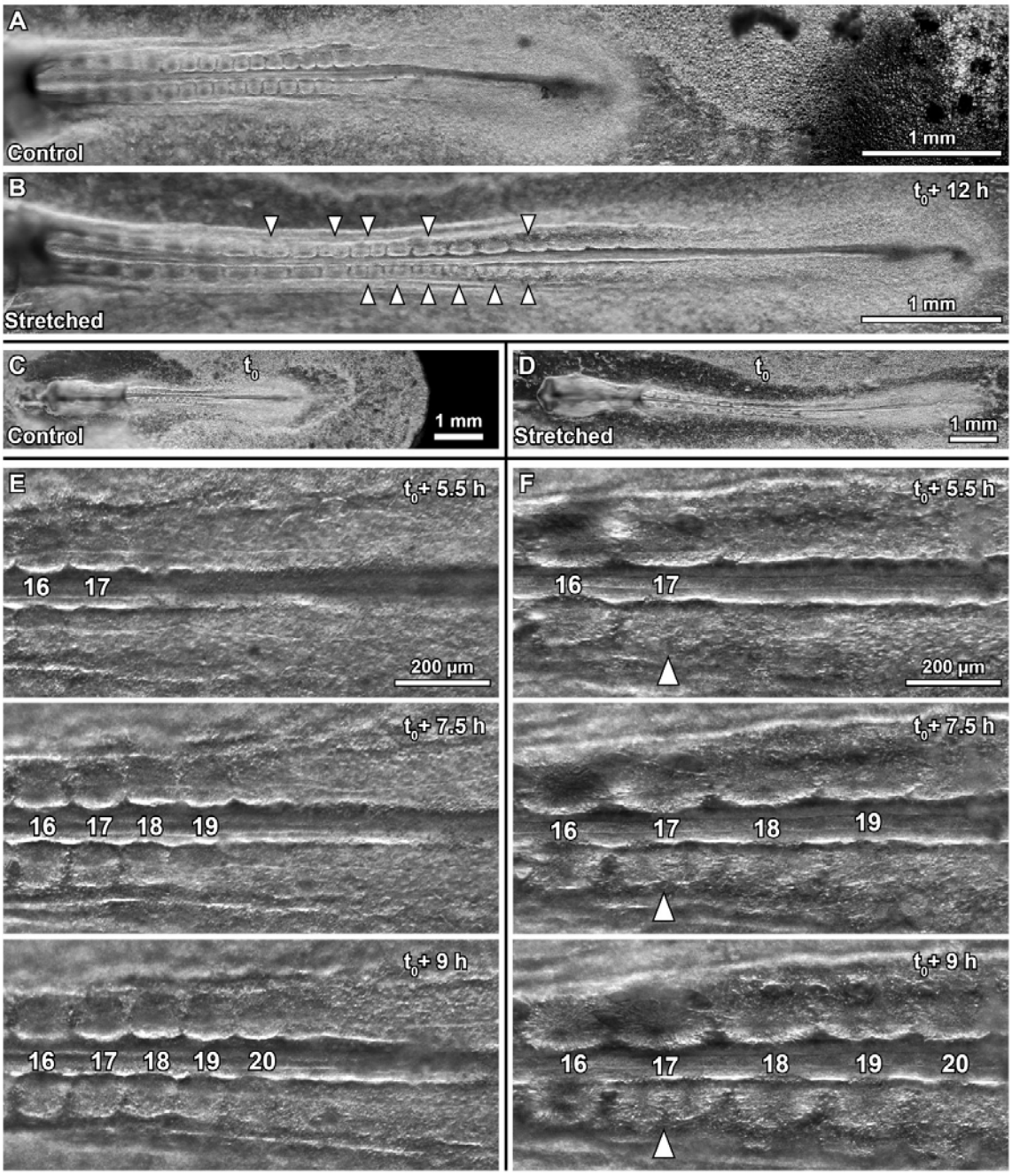

Fig 1: Daughter somite formation in stretched chicken embryos.

Dark-field microscopy images of age-matched (**A**) control and (**B**) stretched embryo. Anterior is to the left in all images, arrowheads indicate divided somites, t_0 = end of stretch protocol, ventral view. Difference in axial length becomes obvious between control embryo (**C**) and stretched embryo (**D**) (t_0: both embryos are at the 13-somite stage). Selected time-lapse

111 frames of the segmenting PSM in control embryo (**E**) and stretched embryo (**F**). White
112 arrowhead indicates daughter somite formation.
113
114 Daughter somites appeared as stable, rounded and clearly separated cellular spheres (Fig 1B).
115 They were morphologically similar to control somites, with epithelial cells organized radially
116 around a somitocoel of mesenchymal cells (compare Fig 2C and G). The daughter somites
117 were enclosed by a fibrous extracellular matrix (ECM) staining positively for fibronectin (Fig
118 S4). While somites in control embryos were rounded (Fig 2A), those in stretched embryos
119 were elongated, while any daughter somites were variable in size (Fig 2B, Fig S4 and Fig S5).
120 Small daughter somites consisting of a few epithelial cells only were also observed (Fig S4).
121 After fixation in transitional stages, the apical actin cortices of somites showed discontinuities
122 along their mediolateral plane, indicating openings of the epithelial sheet under influence of
123 the mechanical deformation (Fig 2D, E and Fig S6). At these locations, mesenchymal
124 somitocoel cells appeared elongated, presumably having undergone mesenchymal-to-
125 epithelial transitions (MET), and were integrated into the existing epithelium (Fig 2E and Fig
126 S6). Upon stretching, there was also strong ectopic expression of *EphA4* in the somitocoels
127 (Fig 2I); this was not present in control embryos (Fig 2H) and indicates stretch-induced MET.
128 During normal somitogenesis, cell-cell signalling between receptor EphA4 in the rostral part
129 of somite S-I and its ligand ephrin B2 in the caudal half of somite S0 has two effects: it
130 induces formation of the somite gap (Watanabe, Sato, Saito, Tadokoro, & Takahashi, 2009),
131 but also establishes epithelialization at somite boundaries by initiating a columnar
132 morphology and cell polarity via apical redistribution of β-catenin (Barrios et al., 2003).
133

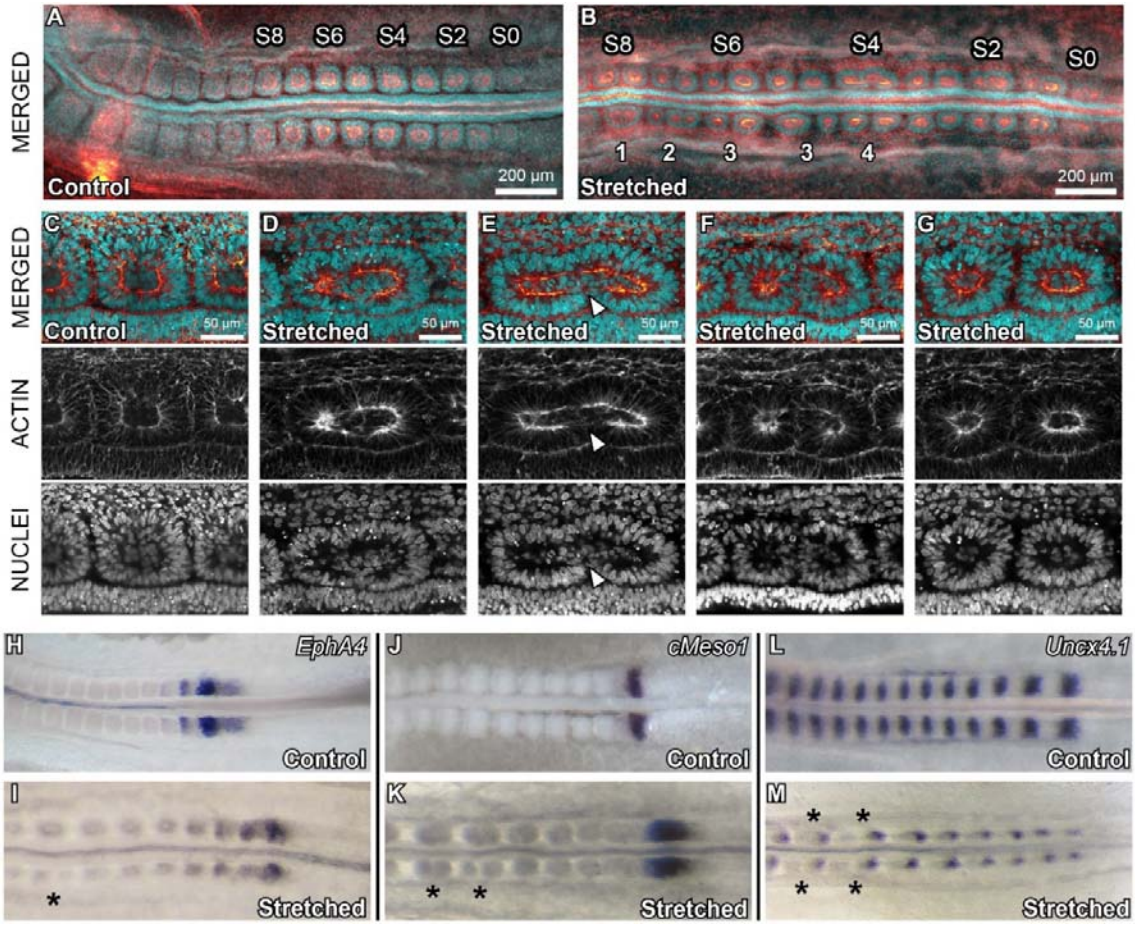

Fig 2: Immunohistochemistry and in situ hybridizations of stretched and control embryos.

Control (A) and stretched embryo (B), anterior is left, somite numbers are indicated (Christ & Ordahl, 1995). Scale bars, 200 µm. (B) Daughter somites can form unilaterally (1), equally (4) or unequally sized (3) and subdivide further (2). (C-G) Confocal cross-sections of selected somites of the same control (C) and stretched embryo (D-G). Anterior is left and medial below. Panels are arranged in potential order to illustrate the transition from a mechanically deformed somite (D) to two daughter somites (G). Cells from the somitocoel seem to gain an elongated morphology, possibly before incorporation into the epithelium (arrowhead in E). (H-M) *In situ* hybridizations for *EphA4, cMeso1* and *Uncx4.1* show that *EphA4* expression is induced around the somitocoels (I), while no new rostro-caudal polarity is induced in the daughter somites (indicated by *).

However, the expression pattern for *cMeso1,* the key initiator of somite rostro-caudal polarity in the unsegmented PSM in chicken (Morimoto et al., 2007), was not influenced by the stretching (Fig 2K), and the expression pattern of caudal somite marker *Uncx4.1* (Schrägle, Huang, Christ, & Pröls, 2004) showed that daughter somites did not gain a new rostro-caudal genetic identity (Fig 2M). Altogether, our data suggest that mechanical stretching did not affect the unsegmented PSM or the rostro-caudal polarization of the somites. However, mechanical stretching did lead to continuation of EphA4-mediated epithelialization of mesenchymal cells from the somitocoel in somites undergoing daughter-somite formation.

To identify the conditions under which mechanically deformed somites would successfully reorganize into daughter somites, we used the Cellular Potts model (CPM) and implemented a cell-based computer simulation with the open-source package CompuCell3D (Glazier & Graner, 1993; Swat et al., 2012). The somite consisted of a core of non-polarized mesenchymal cells surrounded by a layer of polarized, epithelial cells (Dias et al., 2014). We simulated a somite embedded within an elastic extracellular matrix (ECM; Fig 3A) and mimicked stretching by applying axial tension to the ECM (Fig 3B, Movie S3). To narrow down the possible mechanisms for somite reorganization under mechanical deformation, we tested different rules for cellular behaviour in the deformed somite (Fig S10).

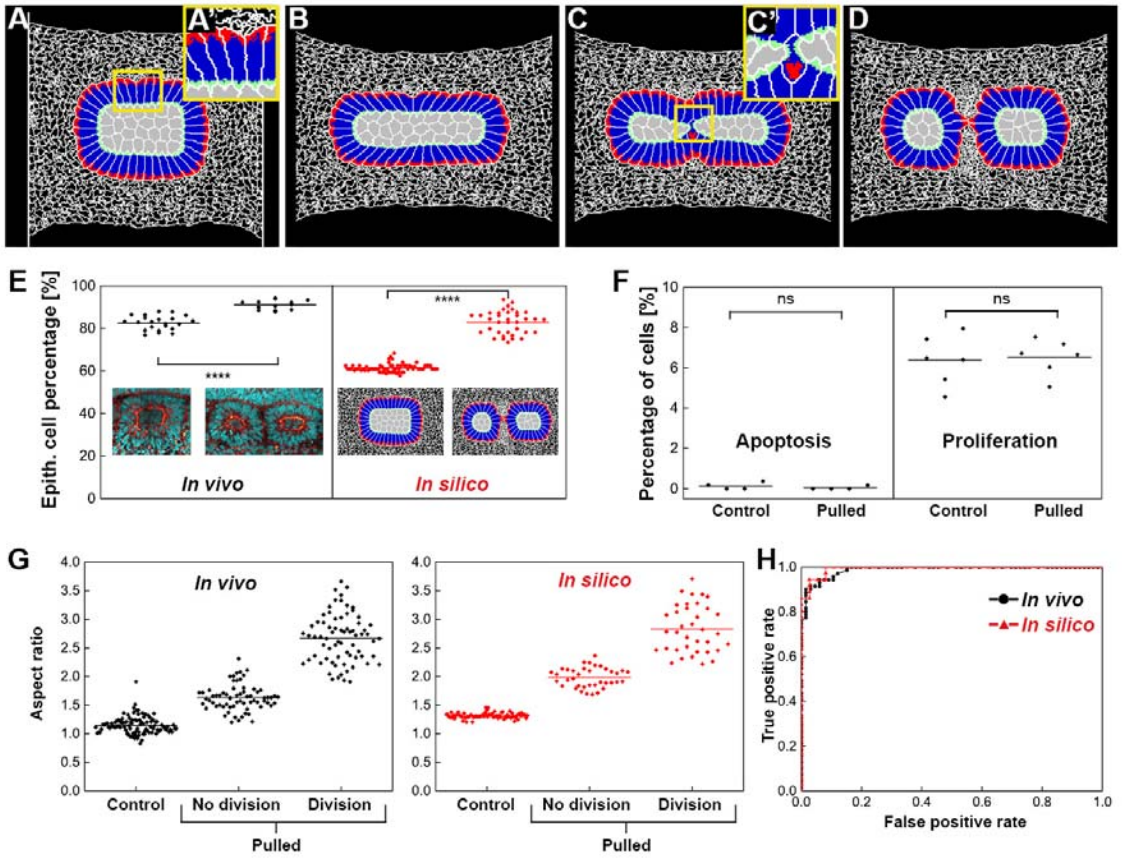

Fig 3: Cellular Potts model of somite remodelling in comparison to daughter somite formation in vivo.

(A-D) Daughter somite formation *in silico*, induced by stretching. Mesenchymal cells (grey) and extracellular matrix (white mesh), (A') epithelial cells consisting of apical (green), lateral (blue) and basal (red) domains. (C') Somitocoel cells undergoing MET. (E) Percentages of epithelial cells in control and divided somites *in silico* and *in vivo*, average line is shown. Significant increase of epithelial cell fraction *in vivo* ($P<0.0001$) and *in silico* ($P<0.0001$). (F) Apoptotic and proliferation rates in somitic mesoderm of control and stretched embryos. Differences non-significant (Mann-Whitney test, apoptosis $P=0.43$, proliferation $P=0.79$). (G) Somite aspect ratios *in vivo* and *in silico*. Point clouds and average lines are given. (H) ROC curves for daughter somite formation *in vivo* and *in silico*, in dependence of aspect ratio of

179 deformed somites. AUC is *0.989* (*in vivo*, 95% CI: 0.953-0.999) and 0.993 (*in silico*, 95% CI:
180 0.938-1.000).
181
182 We found that daughter-somite formation *in silico* could successfully be induced only if MET
183 was initiated when mesenchymal core cells came into contact with the basal or lateral
184 membranes of epithelial cells (Fig 3C, C' and D). To validate this model prediction *in vivo*,
185 we calculated the relative fraction of mesenchymal and epithelial cells in the equatorial cross-
186 section of control somites and divided somites. This showed that the epithelial cell fraction
187 was indeed significantly higher in daughter somites than in controls, and also matched the *in*
188 *silico* prediction independent of the size of the initial somite (Fig 3E, Fig S11). As the
189 stretching *in vivo* caused no significant changes in the apoptosis and proliferation rates (Fig
190 3F), we conclude that the increase in the epithelial cell fraction was due to MET.
191
192 To determine the relationship between mechanical deformation and somite division, we
193 compared the aspect ratios of stretched dividing somites (prior to division) and stretched non-
194 dividing somites with those of control somites (Fig 3G, Fig S7). These measurements show
195 that somite division is only possible beyond an aspect ratio threshold of about 2 *in vivo* or 2.5
196 *in silico*. The corresponding receiver operating characteristics (ROC) curves (Goodenough,
197 Rossmann, & Lusted, 1974; Hanley & McNeil, 1982; Lusted, 1971; Metz, 1978) show that
198 the somite aspect ratio is indeed an excellent predictor of somite division *in vivo* and *in silico*,
199 indicating that daughter-somite formation is a highly mechanically-determined process (Fig
200 3H).
201

Discussion

We found that mechanical stretching of live chick embryos can induce a slow reorganization of somites to form two or more well-shaped and stable daughter somites. The complete division of a stretched somite into daughter somites took several hours, indicating that daughter-somite formation is an active process of tissue reorganization, rather than acute mechanical disruption. The resulting formation of new epithelial borders took place in the somitic mesoderm, *i.e.* outside the functional range of the molecular cues described in the clock-and-wavefront mechanism (Hubaud & Pourquié, 2014). Remarkably, the segmentation clock speed (estimated by the average somite formation time) and the genetic segmentation (A-P-polarity of the somites) stay robust during severe deformations imposed on the embryo. As the FGF/WNT gradients are intracellular by mRNA or protein inheritance (Dubrulle & Pourquié, 2004), the cells may retain their local information, despite their different spacing after stretching. Interestingly, our data show that the organization of forming somites is not final after their separation from the anterior tip of the PSM, but that somites can still adapt to their environment.

High-resolution confocal imaging indicates that, during daughter-somite formation, the demand for additional border cells is satisfied by the recruitment of mesenchymal cells from the somitocoel into the existing epithelium. The mechanical deformation creates discontinuities in the apical actin cortices of stretched somites. At the resulting interfaces, mesenchymal cells from the somite core undergo mesenchymal-epithelial transitions (MET) and get integrated into the somitic epithelium. Similarly, it has been shown previously that the development of normal somitic epithelia involves a continuous addition of cells from the somitocoel by accretion and egression (Martins et al., 2009). Our observations indicate that, by adding mesenchymal cells to the epithelium via a similar cellular behaviour during

227 stretching, the epithelium adapts to the changing environment. Under sufficient deformation,
228 this can lead to daughter-somite formation.
229
230 We were able to model daughter-somite formation *in silico* only if MET was initiated when
231 mesenchymal core cells came into contact with the basal or lateral membranes of epithelial
232 cells. This suggests a contact-induced mechanism triggering MET of somitocoel cells during
233 daughter-somite formation. *In vivo*, we observed ectopic expression of *EphA4* without
234 c*Meso1* expression in strained somites, although *EphA4* is thought to be downstream of
235 c*Meso1* (Watanabe et al., 2009). This indicates that *EphA4* expression in stretched somites is
236 maintained or reinitiated, suggesting an additional mechanosensitive pathway that leads to
237 *EphA4* upregulation during somite division that is independent from, or redundant to, c*Meso1*.
238 A contact-induced MET mechanism, as suggested here for daughter-somite formation, could
239 underlie general epithelial self-organization during development and homeostasis of epithelia
240 under mechanical stress (Jackson, Kim, Balakrishnan, Stuckenholz, & Davidson, 2017;
241 Martins et al., 2009). This cell behaviour could be mediated via epithelial membrane-based
242 signalling (Baum & Georgiou, 2011; Campbell, Casanova, & Skaer, n.d.), for example on the
243 level of Eph and ephrin binding.
244
245 We show that chick somite formation is phenotypically plastic under changing biomechanical
246 conditions. As the geometry of a somite in a stretched embryo predicts with remarkable
247 reliability if it will reorganize into daughter somites or not, daughter-somite formation is
248 highly mechanically determined. This supports the idea that, like temperature, light regime or
249 salinity (Tibblin et al., 2016), mechanical forces can be an additional cue to the induction of
250 different phenotypes of segmental patterning during embryonic development. To further
251 explore the role of mechanical cues in inducing phenotypic plasticity of vertebral numbers, it

will be necessary to study the effect of modified mesodermal patterning in stretched embryos on later embryonic development. Though in principle possible (Nagai, Sezaki, Nakamura, & Sheng, 2014), transplanting stretched embryos back into a host egg could prove technically challenging due to the deformation of the embryos. It may therefore be more promising to transplant daughter somites into host chick embryos in the egg and see how skeletal patterning might be influenced.

It has been suggested that the wide range of vertebral numbers between vertebrate species could have evolved for two reasons: (1) The spatial dissociation between axis regionalisation via *Hox* gene expression and segmentation patterning, and (2) the evolvability of the segmentation clock's period and its relation to the axial growth of the developing embryo (Gomez et al., 2008; Gomez & Pourquie, 2009; Herrgen et al., 2010). However, if the phenotypic plasticity of somite formation shown in our experiments can indeed translate into different vertebral numbers in the later embryo, our findings could indicate an alternative route for vertebrate body plan evolution. Following the 'side-effect hypothesis' (G. B. Müller, 2003), natural selection may act on body proportions, leading to changes in the geometry and mechanical loading of the somitic mesoderm. As an initial by-product, the phenotypic plasticity of somites that we show in our experiments then may lead to increasing somite numbers. Later, maintenance of a consistent alteration of the somite number over generations may then become consolidated at the genetic level by natural selection, i.e. via genetic assimilation (Braendle & Flatt, 2006; Fusco & Minelli, 2010), thus providing robustness to the development of the newly acquired body plan. A correlation between axial growth of the embryo and somite size has been shown in mice (Tam, 1981). While daughter-somite formation may be useful as a source of skeletal variation, it remains to be clarified whether

and how the developing embryo may cope with the missing A-P polarity of the stretch-induced daughter somites.

Daughter-somite formation could also help to explain an interesting phenomenon. Transitional vertebrae, i.e. vertebrae with morphological characteristic of two adjacent spinal regions (for example lumbar area and sacrum), result from incomplete homeotic shifts of axial identity defined by *Hox* gene expression. Generally, as more than one mutation is needed for complete transformations, incomplete homeotic transformations (and therefore transitional vertebrae) are frequent (Alkema, van der Lugt, Bobeldijk, Berns, & van Lohuizen, 1995; Charité, de Graaff, & Deschamps, 1995; Horan, Wu, Wolgemuth, & Behringer, 1994; Kostic & Capecchi, 1994; Li, Kawasumi, Zhao, Moisyadi, & Yang, 2010; Rancourt, Tsuzuki, & Capecchi, 1995; van den Akker et al., 2001; Varela-Lasheras et al., 2011). However, these transitional vertebrae are statistically underrepresented in several amniote species with variable trunk vertebrae numbers, including *Triturus* newts and lizards ((Kaliontzopoulou, Llorente, & Carretero, 2008; Slijepčević, Galis, Arntzen, & Ivanović, 2015), F. Galis, personal communication, October 2017). This suggests a developmental mechanism which favours complete numbers of trunk vertebrae over transitional vertebrae that might hamper mechanical function (Galis et al., 2014b; Slijepčević et al., 2015). Assuming that additional trunk somites form bilaterally via daughter-somite formation, both newly created somites would have the same axial identity as their mother somite, given that the *Hox* identity is determined mainly before the somite is formed, during the earliest stages of somite formation (Carapuço, Nóvoa, Bobola, & Mallo, 2005; Dubrulle, McGrew, & Pourquié, 2001; Mallo, Wellik, & Deschamps, 2010). This would generate vertebrae of similar regional identity with better mechanical performance than that of potentially disadvantageous transitional vertebrae with a different morphology (Galis et al., 2014a).

Somites' self-organizational properties provide a promising basis for further exploration into the physical component of somite formation and the causal role of mechanics in body-plan evolution.

Materials and Methods

Embryo preparation and culture medium

HH8-9 chicken embryos were explanted using filter paper carriers (Chapman, Collignon, Schoenwolf, & Lumsden, 2001) and cultured *ex ovo* as modified submerged filter paper sandwiches (Chapman et al., 2001; Schmitz et al., 2016), in Pannett-Compton (PC) saline (Pannett & Compton, 1924; Schmitz et al., 2016; Voiculescu, Papanayotou, & Stern, 2008), mixed with freshly harvested thin albumen in a 3:2 ratio. Silicone sheets protected embryos in culture from convection of the medium, thereby avoiding damage. Filter paper carriers were prepared as described recently (Schmitz et al., 2016). Additionally, four holes were cut out from corners of the carriers (Fig S1C) to hook the filter paper sandwiches onto the pins of the motorized arms of the stretching setup (Fig S1A).

Stretching protocol, axial deformation and somite deformation

Embryos were exposed to a standardized stretching protocol in a custom-made embryo stretcher (Fig S1C). In two consecutive stretching intervals, a slow displacement of the computer-controlled metal arm (see red arrow in Fig S1) extended the filter paper sandwiches by 3.7 to 3.95 mm at a speed of 1.2 µm/s. At this speed, each stretch took 53 to 55 min. We calculated the mechanical strain for the first and the second stretching as relative length change compared to the axial length before stretching. Results are presented in S1 Table. The first stretch lead to 23 ± 3 % strain (average and standard deviation over all 21 embryos presented in S1 Table). The second pull caused 19 ± 3 % strain. For details on the embryo stretching, somite formation time and determination of somite deformation by aspect ratio, see SI Materials and Methods.

Immunohistochemistry

After the pulling experiments, the embryos and age-matched controls were fixed in 4% paraformaldehyde overnight in PBS at 4°C. Permeabilization in PBST + 0.15% Triton-X-100 lasted for 1.5 hours. Blocking was performed for 2 hours in PBST + 2% BSA + 5% normal goat serum. The following antibody was used: fibronectin mouse-anti-chicken (B3/D6-s, Hybridoma bank). The antibody was diluted in PBST with 1% BSA. Embryos were incubated in primary antibody solution for 24h at 4°C, followed by extensive washing in PBS and incubation with appropriate Alexa Fluor-conjugated secondary antibody (1:500, Molecular Probes). Embryos were stained for F-actin using Alexa Fluor 546 Phalloidin (1:200, Molecular Probes) and for nucleic DNA using DAPI (1 µg/ml). Cell proliferation and apoptosis staining was performed using following antibodies: rabbit polyclonal anti-cleaved caspase-3 (1:200, Cell Signaling) and rabbit polyclonal anti-phosphohistone-H3 (1:400, Cell Signaling) with the appropriate Alexa Fluor-conjugated secondary antibodies (1:500, Invitrogen) and DAPI for nucleic DNA (1 µg/ml). For details on mesenchymal and epithelial cell counts, see SI Materials and Methods.

In situ hybridizations

In situ hybridizations were performed by standard procedures. Embryos were fixated in freshly prepared 4 % PFA in PBS. The embryos were pre-treated with proteinase-K in PBST at 37°C with agitation for 3 minutes. During staining, embryos were incubated in NTMT containing 4.5 µl NBT (75mg/ml in 70% DMF) and 3.5 µl BCIP (50mg/ml in 100% DMF) per 1.5 ml. Pulled embryos and age-matched controls were stained in the same wells for the same time, as much as possible. After the staining had been stopped, the embryos were

photographed in glycerol 80% in H_2O with a Leica DFC320 camera on a Leica MZ75 microscope.

Cellular Potts model of somite division

To understand the influence of mechanical stretching on somites and the somite division observed *in vivo*, we constructed a two-dimensional mathematical model based on the Cellular Potts Model (Glazier & Graner, 1993; Graner & Glazier, 1992), representing a cross-section through a three-dimensional somitic tissue. For the modelling details, see SI Materials and Methods.

Acknowledgements

We are grateful to Julio Belmonte for his advice on the simulations at the early stages of model development. We thank Stuart A. Newman and Frietson Galis for valuable comments during the final preparation of the manuscript.

Competing interests

The authors declare that there are no conflicts of interest.

Author Contributions

B.N. and M.S. performed the experiments and analysed the data. H.T. and R.M. performed the simulations. T.S. and R.M. supervised the project. All authors wrote the manuscript.

References

Alkema, M. J., van der Lugt, N. M., Bobeldijk, R. C., Berns, A., & van Lohuizen, M. (1995). Transformation of axial skeleton due to overexpression of bmi-1 in transgenic mice. *Nature*, *374*(6524), 724–7. https://doi.org/10.1038/374724a0

Barrios, A., Poole, R. J., Durbin, L., Brennan, C., Holder, N., & Wilson, S. W. (2003). Eph / Ephrin Signaling Regulates the Mesenchymal- to-Epithelial Transition of the Paraxial Mesoderm during Somite Morphogenesis. *Current Biology*, *13*, 1571–1582. https://doi.org/10.1016/j

Baum, B., & Georgiou, M. (2011). Dynamics of adherens junctions in epithelial establishment, maintenance, and remodeling. *Journal of Cell Biology*, *192*(6), 907–917. https://doi.org/10.1083/jcb.201009141

Beacham, T. D., & Murray, C. B. (1986). The Effect of Spawning Time and Incubation Temperature on Meristic Variation in Chum Salmon Oncorhynchus-Keta. *Canadian Journal of Zoology*, *64*(1), 45–48.

Braendle, C., & Flatt, T. (2006). A role for genetic accommodation in evolution? *BioEssays*. https://doi.org/10.1002/bies.20456

Campbell, K., Casanova, J., & Skaer, H. (n.d.). Mesenchymal-to-epithelial transition of intercalating cells in Drosophila renal tubules depends on polarity cues from epithelial neighbours. *Mechanisms of Development*, *127*(7–8), 345–57. https://doi.org/10.1016/j.mod.2010.04.002

Carapuço, M., Nóvoa, A., Bobola, N., & Mallo, M. (2005). Hox genes specify vertebral types in the presomitic mesoderm. *Genes and Development*, *19*(18), 2116–2121. https://doi.org/10.1101/gad.338705

Chal, J., Guillot, C., & Pourquié, O. (2016). PAPC couples the Segmentation Clock to somite morphogenesis by regulating N-cadherin dependent adhesion. *bioRxiv*.

https://doi.org/10.1101/071084

Chapman, S. C., Collignon, J., Schoenwolf, G. C., & Lumsden, A. (2001). Improved method for chick whole-embryo culture using a filter paper carrier. *Developmental Dynamics*, *220*(3), 284–289. https://doi.org/10.1002/1097-0177(20010301)220:3<284::AID-DVDY1102>3.0.CO;2-5

Charité, J., de Graaff, W., & Deschamps, J. (1995). Specification of multiple vertebral identities by ectopically expressed Hoxb-8. *Developmental Dynamics : An Official Publication of the American Association of Anatomists*, *204*(1), 13–21. https://doi.org/10.1002/aja.1002040103

Christ, B., & Ordahl, C. P. (1995). Early stages of chick somite development. *Anatomy and Embryology*, *191*(5), 381–396. Retrieved from http://www.ncbi.nlm.nih.gov/pubmed/7625610

Dias, A. S., de Almeida, I., Belmonte, J. M., Glazier, J. A., & Stern, C. D. (2014). Somites Without a Clock. *Science*, *343*(6172), 791–795. https://doi.org/10.1126/science.1247575

Dubrulle, J., McGrew, M. J., & Pourquié, O. (2001). FGF signaling controls somite boundary position and regulates segmentation clock control of spatiotemporal Hox gene activation. *Cell*, *106*(2), 219–232. https://doi.org/10.1016/S0092-8674(01)00437-8

Dubrulle, J., & Pourquié, O. (2004). fgf8 mRNA decay establishes a gradient that couples axial elongation to patterning in the vertebrate embryo. *Nature*, *427*(6973), 419–22. https://doi.org/10.1038/nature02216

Duess, J. W., Fujiwara, N., Corcionivoschi, N., Puri, P., & Thompson, J. (2013). ROCK inhibitor (Y-27632) disrupts somitogenesis in chick embryos. *Pediatric Surgery International*, *29*(1), 13–8. https://doi.org/10.1007/s00383-012-3202-7

Fusco, G., & Minelli, A. (2010). Phenotypic plasticity in development and evolution: facts and concepts. *Philosophical Transactions of the Royal Society B: Biological Sciences*,

427 *365*(1540), 547–556. https://doi.org/10.1098/rstb.2009.0267

428 Galis, F., Carrier, D. R., van Alphen, J., van der Mije, S. D., Van Dooren, T. J. M., Metz, J. A.
429 J., & ten Broek, C. M. A. (2014a). Fast running restricts evolutionary change of the
430 vertebral column in mammals. *Proceedings of the National Academy of Sciences*,
431 *111*(31), 11401–11406. https://doi.org/10.1073/pnas.1401392111

432 Galis, F., Carrier, D. R., van Alphen, J., van der Mije, S. D., Van Dooren, T. J. M., Metz, J. A.
433 J., & ten Broek, C. M. A. (2014b). Fast running restricts evolutionary change of the
434 vertebral column in mammals. *Proceedings of the National Academy of Sciences*,
435 *111*(31), 11401–11406. https://doi.org/10.1073/pnas.1401392111

436 Glazier, & Graner. (1993). Simulation of the differential adhesion driven rearrangement of
437 biological cells. *Physical Review. E, Statistical Physics, Plasmas, Fluids, and Related*
438 *Interdisciplinary Topics*, *47*(3), 2128–2154. Retrieved from
439 http://www.ncbi.nlm.nih.gov/pubmed/9960234

440 Gomez, C., Ozbudak, E. M., Wunderlich, J., Baumann, D., Lewis, J., & Pourquié, O. (2008).
441 Control of segment number in vertebrate embryos. *Nature*, *454*(7202), 335–339.
442 https://doi.org/10.1038/nature07020

443 Gomez, C., & Pourquie, O. (2009). Developmental control of segment numbers in vertebrates.
444 *Journal of Experimental Zoology Part B: Molecular and Developmental Evolution*,
445 *312*(6), 533–544. https://doi.org/10.1002/jez.b.21305

446 Goodenough, D. J., Rossmann, K., & Lusted, L. B. (1974). Radiographic applications of
447 receiver operating characteristic (ROC) curves. *Radiology*, *110*(1), 89–95.
448 https://doi.org/10.1148/110.1.89

449 Graner, F., & Glazier, J. A. (1992). Simulation of Biological Cell Sorting Using a 2-
450 Dimensional Extended Potts-Model. *Physical Review Letters*, *69*(13), 2013–2016.
451 https://doi.org/10.1103/PhysRevLett.69.2013

452 Hamburger, V., & Hamilton, H. L. (1951). A series of normal stages in the development of
453 the chick embryo. *Journal of Morphology*, *88*(1), 49–92.
454 https://doi.org/10.1002/jmor.1050880104
455 Hanley, A. J., & McNeil, J. B. (1982). The Meaning and Use of the Area under a Receiver
456 Operating Characteristic (ROC) Curve. *Radiology*, *143*, 29–36.
457 https://doi.org/10.1148/radiology.143.1.7063747
458 Herrgen, L., Ares, S., Morelli, L. G., Schröter, C., Jülicher, F., & Oates, A. C. (2010).
459 Segment Number and Axial Identity in a Segmentation Clock Period Mutant. *Current*
460 *Biology*, *20*(14), 1254–1258. https://doi.org/10.1016/j.cub.2010.05.071
461 Horan, G. S., Wu, K., Wolgemuth, D. J., & Behringer, R. R. (1994). Homeotic transformation
462 of cervical vertebrae in Hoxa-4 mutant mice. *Proceedings of the National Academy of*
463 *Sciences of the United States of America*, *91*(26), 12644–8. Retrieved from
464 http://www.ncbi.nlm.nih.gov/pubmed/7809093
465 Horikawa, K., Radice, G., Takeichi, M., & Chisaka, O. (1999). Adhesive Subdivisions
466 Intrinsic to the Epithelial Somites. *In Situ*, *215*, 182–189.
467 https://doi.org/10.1006/dbio.1999.9463
468 Hubaud, A., & Pourquié, O. (2014). Signalling dynamics in vertebrate segmentation. *Nature*
469 *Reviews Molecular Cell Biology*, *15*(11), 709–721. https://doi.org/10.1038/nrm3891
470 Hubaud, A., Regev, I., Mahadevan, L., & Pourquié, O. (2017). Excitable Dynamics and Yap-
471 Dependent Mechanical Cues Drive the Segmentation Clock. *Cell*.
472 https://doi.org/10.1016/j.cell.2017.08.043
473 Hubbs, C. L. (1922). Variations in the Number of Vertebrae and Other Meristic Characters of
474 Fishes Correlated with the Temperature of Water during Development. *The American*
475 *Naturalist*, *56*(645), 360. https://doi.org/10.1086/279875
476 Jackson, T. R., Kim, H. Y., Balakrishnan, U. L., Stuckenholz, C., & Davidson, L. A. (2017).

Spatiotemporally Controlled Mechanical Cues Drive Progenitor Mesenchymal-to-Epithelial Transition Enabling Proper Heart Formation and Function. *Current Biology : CB*, *27*(9), 1326–1335. https://doi.org/10.1016/j.cub.2017.03.065

Jockusch, E. L. (1997). Geographic variation and phenotypic plasticity of number of trunk vertebrae in Slender Salamanders, Batrachoseps (Caudata: Plethodontidae). *Evolution*, *51*(6), 1966–1982. https://doi.org/10.2307/2411017

Kaliontzopoulou, A., Llorente, G., & Carretero, M. (2008). Interspecific and intersexual variation in presacral vertebrae number in Podarcis bocagei and P. carbonelli. *Amphibia-Reptilia*, *29*(2), 288–292. https://doi.org/10.1163/156853808784125018

Kimura, Y., Matsunami, H., Inoue, T., Shimamura, K., Uchida, N., Ueno, T., … Takeichi, M. (1995). Cadherin-11 expressed in association with mesenchymal morphogenesis in the head, somite, and limb bud of early mouse embryos. *Developmental Biology*. https://doi.org/10.1006/dbio.1995.1149

Kostic, D., & Capecchi, M. R. (1994). Targeted disruptions of the murine Hoxa-4 and Hoxa-6 genes result in homeotic transformations of components of the vertebral column. *Mechanisms of Development*, *46*(3), 231–47. Retrieved from http://www.ncbi.nlm.nih.gov/pubmed/7918106

Kulesa, P. M., Schnell, S., Rudloff, S., Baker, R. E., & Maini, P. K. (2007). From segment to somite: Segmentation to epithelialization analyzed within quantitative frameworks. *Developmental Dynamics*, *236*(May), 1392–1402. https://doi.org/10.1002/dvdy.21199

Laland, K. N., Uller, T., Feldman, M. W., Sterelny, K., Müller, G. B., Moczek, A., … Odling-Smee, J. (2015). The extended evolutionary synthesis: its structure, assumptions and predictions. *Proceedings of the Royal Society B: Biological Sciences*, *282*(1813), 20151019. https://doi.org/10.1098/rspb.2015.1019

Lecyk, M. (1966). The effect of hyperthermia applied in the given stages of pregnancy on the

number and form of vertebrae in the offspring of white mice. *Experientia*, *22*(4), 254–255. https://doi.org/10.1007/BF01900945

Li, Z., Kawasumi, M., Zhao, B., Moisyadi, S., & Yang, J. (2010). Transgenic over-expression of growth differentiation factor 11 propeptide in skeleton results in transformation of the seventh cervical vertebra into a thoracic vertebra. *Molecular Reproduction and Development*, *77*(11), 990–7. https://doi.org/10.1002/mrd.21252

Lindsey, C. C., & Moodie, G. E. E. (1967). THE EFFECT OF INCUBATION TEMPERATURE ON VERTEBRAL COUNT IN THE CHICKEN. *Canadian Journal of Zoology*, *45*(5), 891–892. https://doi.org/10.1139/z67-099

Lusted, L. B. (1971). Decision-making studies in patient management. *New England Journal of Medicine*, *284*(8), 416–424. https://doi.org/10.1056/nejm197102252840805

Mallo, M., Wellik, D. M., & Deschamps, J. (2010). Hox genes and regional patterning of the vertebrate body plan. *Developmental Biology*. https://doi.org/10.1016/j.ydbio.2010.04.024

Marmottant, P., Mgharbel, A., Kafer, J., Audren, B., Rieu, J.-P., Vial, J.-C., … Delanoe-Ayari, H. (2009). The role of fluctuations and stress on the effective viscosity of cell aggregates. *Proceedings of the National Academy of Sciences of the United States of America*, *106*(41), 17271–17275. https://doi.org/10.1073/pnas.0902085106

Martins, G. G., Rifes, P., Amândio, R., Rodrigues, G., Palmeirim, I., & Thorsteinsdóttir, S. (2009). Dynamic 3D cell rearrangements guided by a fibronectin matrix underlie somitogenesis. *PloS One*, *4*(10), e7429. https://doi.org/10.1371/journal.pone.0007429

Metz, C. E. (1978). Basic principles of ROC analysis. *Seminars in Nuclear Medicine*, *8*(4), 283–298. https://doi.org/http://dx.doi.org/10.1016/S0001-2998(78)80014-2

Morimoto, M., Sasaki, N., Oginuma, M., Kiso, M., Igarashi, K., Aizaki, K., … Saga, Y. (2007). The negative regulation of Mesp2 by mouse Ripply2 is required to establish the

527 rostro-caudal patterning within a somite. *Development (Cambridge, England)*, *134*(8),
528 1561–9. https://doi.org/10.1242/dev.000836
529 Müller, G. (1990). The origin of evolutionary novelties: a side-effect hypothesis. In M. H.
530 Nitecki & D. V. Nitecki (Eds.), *Evolutionary innovations* (pp. 99–130). Retrieved from
531 https://books.google.com/books?hl=en&lr=&id=2nUGkIXMR58C&pgis=1
532 Müller, G. B. (2003). Embryonic motility: Environmental influences and evolutionary
533 innovation. *Evolution and Development*, *5*(1), 56–60. https://doi.org/10.1046/j.1525-
534 142X.2003.03009.x
535 Nagai, H., Sezaki, M., Nakamura, H., & Sheng, G. (2014). Extending the limits of avian
536 embryo culture with the modified Cornish pasty and whole-embryo transplantation
537 methods. *Methods*, *66*(3), 441–446. https://doi.org/10.1016/j.ymeth.2013.05.005
538 Newman, M. E. J., & Barkema, G. T. (1999). *Monte Carlo Methods in Statistical Physics*.
539 Clarendon Press Oxford.
540 Osgood, D. W. (1978). Effects of temperature on the development of meristic characters in
541 Natrix fasciata. *Copeia*, *1978*(1), 33–47.
542 P.Rifes, thesis: Fibronectin cues during somite formation, Universidade de Lisboa (2013).
543 (n.d.).
544 Pannett, C., & Compton, A. (1924). the Cultivation of Tissues in Saline Embryonic Juice. *The*
545 *Lancet*, *203*(5243), 381–384. https://doi.org/10.1016/S0140-6736(01)15954-4
546 Peabody, R. B., & Brodie Jr., E. D. (1975). Effect of Temperature, Salinity and Photoperiod
547 on the Number of Trunk Vertebrae in Ambystoma maculatum. *Copeia*, *1975*(4), 741–
548 746. https://doi.org/10.2307/1443326
549 Rancourt, D. E., Tsuzuki, T., & Capecchi, M. R. (1995). Genetic interaction between hoxb-5
550 and hoxb-6 is revealed by nonallelic noncomplementation. *Genes & Development*, *9*(1),
551 108–22. Retrieved from http://www.ncbi.nlm.nih.gov/pubmed/7828847

552 Richardson, M. K., Allen, S. P., Wright, G. M., Raynaud, a, & Hanken, J. (1998). Somite
553 number and vertebrate evolution. *Development (Cambridge, England)*, *125*, 151–160.
554 Schmitz, M., Nelemans, B. K. A., & Smit, T. H. (2016). A Submerged Filter Paper Sandwich
555 for Long-term Ex Ovo Time-lapse Imaging of Early Chick Embryos, (118), e54636.
556 https://doi.org/doi:10.3791/54636
557 Schrägle, J., Huang, R., Christ, B., & Pröls, F. (2004). Control of the temporal and spatial
558 Uncx4.1 expression in the paraxial mesoderm of avian embryos. *Anatomy and*
559 *Embryology*, *208*(4), 323–32. https://doi.org/10.1007/s00429-004-0404-3
560 Slijepčević, M., Galis, F., Arntzen, J. W., & Ivanović, A. (2015). Homeotic transformations
561 and number changes in the vertebral column of Triturus newts. *PeerJ*, *3*(11), e1397.
562 https://doi.org/10.7717/peerj.1397
563 Stern, C. D., & Bellairs, R. (1984). The roles of node regression and elongation of the area
564 pellucida in the formation of somites in avian embryos. *Journal of Embryology and*
565 *Experimental Morphology*, *81*, 75–92.
566 Swat, M. H., Thomas, G. L., Belmonte, J. M., Shirinifard, A., Hmeljak, D., & Glazier, J. A.
567 (2012). Multi-Scale Modeling of Tissues Using CompuCell3D. *Methods in Cell Biology*,
568 *110*, 325–366. https://doi.org/10.1016/B978-0-12-388403-9.00013-8
569 Tahir, H., Niculescu, I., Bona-Casas, C., Merks, R. M. H., & Hoekstra, A. G. (2015). An in
570 silico study on the role of smooth muscle cell migration in neointimal formation after
571 coronary stenting. *Journal of The Royal Society Interface*, *12*(108).
572 Tam, P. P. (1981). The control of somitogenesis in mouse embryos. *Journal of Embryology*
573 *and Experimental Morphology*, *65 Suppl*, 103–128.
574 Tibblin, P., Berggren, H., Nordahl, O., Larsson, P., & Forsman, A. (2016). Causes and
575 consequences of intra-specific variation in vertebral number. *Scientific Reports*, *6*(April),
576 26372. https://doi.org/10.1038/srep26372

van den Akker, E., Fromental-Ramain, C., de Graaff, W., Le Mouellic, H., Brûlet, P., Chambon, P., & Deschamps, J. (2001). Axial skeletal patterning in mice lacking all paralogous group 8 Hox genes. *Development (Cambridge, England)*, *128*(10), 1911–21. Retrieved from http://www.ncbi.nlm.nih.gov/pubmed/11311170

Varela-Lasheras, I., Bakker, A. J., van der Mije, S. D., Metz, J. A., van Alphen, J., & Galis, F. (2011). Breaking evolutionary and pleiotropic constraints in mammals: On sloths, manatees and homeotic mutations. *EvoDevo*, *2*(1), 11. https://doi.org/10.1186/2041-9139-2-11

Voiculescu, O., Papanayotou, C., & Stern, C. D. (2008). Spatially and temporally controlled electroporation of early chick embryos. *Nat Protoc*, *3*(3), 419–426. https://doi.org/nprot.2008.10 [pii]\r10.1038/nprot.2008.10

Watanabe, T., Sato, Y., Saito, D., Tadokoro, R., & Takahashi, Y. (2009). EphrinB2 coordinates the formation of a morphological boundary and cell epithelialization during somite segmentation. *Proceedings of the National Academy of Sciences of the United States of America*, *106*(18), 7467–72. https://doi.org/10.1073/pnas.0902859106

Supporting Information

SI Materials and Methods

Egg handling

Fertilized chicken eggs, white-leghorn, *Gallus gallus domesticus* (Linnaeus, 1758), were obtained from Drost B.V. (Loosdrecht, The Netherlands), incubated at 37,5°C in a moist atmosphere, and automatically turned every hour. After incubation for approx. 33 h, HH8-9 embryos were explanted using filter paper carriers (Chapman et al., 2001) and cultured *ex ovo* as modified submerged filter paper sandwiches (Chapman et al., 2001; Schmitz et al., 2016)

Culture medium

Embryo culture medium consisted of Pannett-Compton (PC) saline (Pannett & Compton, 1924; Schmitz et al., 2016; Voiculescu et al., 2008), mixed with freshly harvested thin albumen in a 3:2 ratio. PC stock solutions can be stored at 4 ^{0}C for several months, but PC saline (mixture of stock solutions and MilliQ-water) should be prepared freshly every week and stored at 4^{0}C between experiments. Addition of Penicillin/Streptomycin (10000 U/ml) in 100x dilution prevents occasionally appearing bacterial infections.

Silicone sheets

Silicone sheets protected embryos in culture from convection of the medium, thereby avoiding additional damage. Silicone sheets (ca. 350 µm in thickness) were made using a Sylgard® 184 Silicone Elastomer Kit as follows: A 15-cm plastic petri dish was placed on a scale and 6.165 g (5.554 mL) of base solution were pipetted into its center using a plastic transfer pipette (cut off tip). Then 0.206 g (0.2 mL) of curing agent were added using a glass

pipette. Base and curing agent were mixed slowly, using a wooden spatula and spread out over the bottom of the petri dish. The petri dish was placed into a vacuum chamber for 2 hrs to remove air bubbles and let silicone solution spread out equally. Exposure to 80 °C for ca. 2 hrs let silicone polymerize and cure. Afterwards, silicone was let to cool to room temperature for about 5 hrs or overnight. Tweezers were used to free the borders of the silicone sheet from the walls of the petri dish and peel the sheet from the culture dish (wear gloves). Silicone was stored between sheets of a plastic document sleeve to prevent accumulation of dust. For preparing silicone sheets fitting in the setup, the plastic sleeve was removed from one side of the silicone sheet and the plastic stencil (Fig S1D) placed on it. A razor blade was used to cut around the outline of the stencil and the ten holes indicated by the stencil were cut out using a hole puncher. After removing the other plastic sleeve layer, silicone sheets were stored in a closed 10 cm petri dish.

Filter paper carriers

Filter paper carriers were prepared as described recently (Schmitz et al., 2016). Additionally, four holes were cut out from corners of the carriers (Fig S1C) to hook the filter paper sandwiches onto the pins of the motorized arms of the stretching setup (Fig S1A).

Experimental setup - Embryo stretcher

Embryos were cultured and mechanically manipulated on a custom-made embryo stretcher (Fig S1C). This setup allows to culture up to three embryos simultaneously in a variant of the recently described “submerged filter paper sandwich” (Schmitz et al., 2016). The setup consisted of a temperature-controlled medium container/ beaker surrounded by a metal frame. This frame carried two motorized translation stages mounted on opposing sides of the frame. Both stages could be operated with a manual controller. For one of the stages the control

could be switched to a custom-made LabVIEW routine. This routine allowed to define different automated pulling profiles for overnight experiments (see section 'Stretching protocol'). Each stage carried a metal arm reaching into the medium container. Each metal arm ended with a horizontal platform equipped with three arrays of four smooth pins surrounding a threaded pin. The smooth pins functioned as hooks for the filter paper sandwiches and as a guide for metal washers clamping the filter paper sandwiches to the metal arms. Embryos were cultured fully submerged in the culture medium described above and the setup was prepared for an experiment as follows: The temperature-controlled beaker was placed in the center of the motorized x-y-stage of the upright zoom microscope. Then the frame carrying the two motorized translational stages was placed around the temperature-controlled beaker and fixed it with two lateral screws (Fig S1B). The two metal arms were attached to the motorized translational stages and fixed with the screws from top. Using the manual control, the position of the metal arms was adjusted so that the gap between them was 12 mm, by bringing the left translational stage furthest to the right and the right translational stage furthest to the left. Then the temperature controlled beaker was filled with 200 mL of clean culture medium. Any dirt or bubbles were removed from the culture medium using a plastic transfer pipette. If necessary, the culture medium level was adjusted to make sure that the pins on the metal arms were just submerged. The temperature of the temperature-controlled beaker was set to 40°C.Then the silicone sheets were placed into the setup by using the blunt end of tweezers to hook the silicone sheets into the pins of the metal arms. Air bubbles were removed with a plastic transfer pipette. Then a chick embryo was explanted into a filter paper sandwich (Schmitz et al., 2016) (Fig S1A), immediately submerged into the culture medium and hooked it into the innermost pins of both metal arms by pushing it down with the tweezers (Fig S1A The metal washers (Fig S1A and Fig S1E for dimensions) were placed over the pins of both metal arms and gently fixed by nuts using an Inbus® key (Fig

667 S1A). After successfully clamping three filter paper sandwiches into the setup, each filter
668 paper sandwich was cut perpendicularly to the embryonic axis, about 1 mm posteriorly of the
669 widest point of the elliptical aperture (dashed red line in Fig S1A-9). Iris scissors were used
670 for these cuts. Then the surface of the culture medium was covered with 50 mL of light
671 mineral oil using a plastic transfer pipette (Fig S1A-10). Note: After placing the mineral oil,
672 the experiment is set and embryos cannot be replaced anymore without cleaning the whole
673 setup. 25 mL of culture medium were removed from below the oil layer by pinching a plastic
674 transfer pipette through the oil layer into the culture medium and the time-lapse acquisition
675 was set up as described before (Schmitz et al., 2016).
676
677 **Stretching protocol**
678 Embryos were exposed to a standardized stretching protocol which, in preliminary
679 experiments, had proved to cause a strong deformation of the embryos' paraxial mesoderm
680 without impairing the progression of development. The protocol started with a waiting period
681 of 3.5 hrs after covering the culture medium with light mineral oil. This allowed damage,
682 caused during preparation of the filter paper sandwich and perpendicular cutting, to heal.
683 Then, two consecutive stretching intervals followed, separated by a pause of two hours to
684 allow recovery of damaged tissue. Each stretching interval consisted of a slow displacement
685 of the computer controlled metal arm (see red arrow in Fig S1) by 3.7 to 3.95 mm at a speed
686 of 1.2 µm/s. At this speed, each stretch took 53 to 55 min. Fig S2 depicts the user interface of
687 the LabVIEW routine, prepared for an overnight experiment. Travel direction (left or right),
688 speed (to be chosen from a 16-bit range defined by the microcontroller, where 40 equals 1.2
689 µm/s) and time interval (in seconds) could be chosen independently for each experimental
690 block.
691

692 **Macroscopic axial deformation**

693 The macroscopic axial deformation of the stretched embryos was determined by measuring
694 their length from tip of the head to the posterior end of the sinus rhomboidalis, using the
695 segmented line tool in ImageJ (white line in Fig S3A, B, E, F). We assumed that, during the
696 application of the stretching, the natural morphogenetic changes of the embryos are negligible
697 and length changes result from the external stretching only. We calculated the mechanical
698 strain for the first and the second stretching as relative length change compared to the axial
699 length before stretching. Results are presented in S1 Table. The first stretch lead to 23 ± 3 %
700 strain (average and standard deviation over all 21 embryos presented in S1 Table). The second
701 pull caused 19 ± 3 % strain.

702

703 **Somite formation time**

704 The separation of a newly forming somite from the anterior tip of the PSM and its
705 epithelialization is a continuous process involving complex cellular rearrangements lasting
706 longer than the 90 min usually stated to be characteristic for chick embryos (Martins et al.,
707 2009). Nevertheless, we tried to assess the influence of mechanical deformation on
708 somitogenesis by determining an average somite formation rate for stretched and control
709 embryos using our dark field microscopic time-lapse movies and based our calculations on the
710 physical separation of somites from the PSM. We counted the number of somites in stretched
711 embryos at the end of the second pull and at the end of the experiment. If a somite had not
712 completely separated from the PSM at the end of the second pull, the counting was started
713 after formation of the following somite. From the total number of somites formed after the
714 application of the second pull and the corresponding time interval we calculated the somite
715 formation rate. The somite formation rate for control embryos was determined accordingly
716 from the beginning of the culturing in the submerged filter paper sandwich. We did not

observe any difference in somite formation rate between stretched embryos with or without daughter formation or in comparison to non-stretched control embryos (S2 Table).

Proliferation rate and apoptotic rate

Apoptotic (Cas3 staining, control n=4, pulled n=4 embryos) and proliferating (pHH3 staining, control n=6, pulled n=6 embryos) cells in somitic mesoderm lanes (somite S1 to S5) were counted in high-resolution confocal micrographs acquired on a Leica SP8 confocal microscope. At least 500 cells were counted per embryo. Apoptotic rate and proliferation rate were calculated as follows: (apoptotic/proliferation) rate (%) = number of positive staining cells/number of total cells×100. Statistical analysis was performed using GraphPad Prism software. Mann–Whitney unpaired non-parametric two-tail testing was applied to determine the P-values for the apoptotic and proliferation rates shown in Fig 3F. Control and pulled somitic mesoderm showed no significant differences in apoptotic (P=0.4286) and proliferation (P=0.7879) rates.

Epithelial cell percentages

The percentage of epithelial cells in the equatorial z-plane of 13 daughter somite pairs, originating from the same mother somite, and 22 control somites was determined (*in vivo)*. To that end, high-resolution confocal micrographs of embryos stained with DAPI for nucleic DNA were acquired on a Leica SP8 confocal microscope. Then somites were counted for (mesenchymal) core cells and epithelial cells to calculate epithelial cell percentages. *In silico,* cell percentages in 12 daughter somite pairs and 12 control somites were counted accordingly. Statistical analysis was performed using GraphPad Prism software. Unpaired parametric two tailed t-tests (with Welch's correction for unequal variance) were applied to determine P-

741 values for the epithelial percentages shown in the graph in Fig 3E. The percentages of
742 epithelial cells change significantly *in vivo* (P<0,0001) and *in silico* (P<0,0001).
743
744
745 **Aspect ratio determination and ROC curve**
746 The geometry of somites *in vivo* in controls and stretched embryos was described by
747 measuring their length in rostro-caudal (x) and their width in medio-lateral (y) direction using
748 the "Measure"-tool in ImageJ. Subsequently, the corresponding aspect ratio AR (AR = x/y)
749 was calculated. Somites forming in controls and in stretched embryos after the second pull
750 were measured upon their separation from the anterior tip of the PSM (Fig S7A-B). Somites
751 that had been formed before were measured at the end of the second pull (Fig S7C). The
752 aspect ratio of somites *in silico* was determined before (Fig S7D) and after the application of
753 the pull (Fig S7E) accordingly (for strain regimes *in silico* see below). The corresponding
754 receiver operating characteristics (ROC) curves (Goodenough et al., 1974; Hanley & McNeil,
755 1982; Lusted, 1971; Metz, 1978) (Fig 3H) were generated by performing a binary logistic
756 regression using the Data Analysis Tool of the Real Statistics Excel plugin Realstats
757 (available at http://www.real-statistics.com). We analyzed how well the aspect ratio of
758 stretched somites *in vivo* and *in silico* can predict the binary outcome of whether a somite will
759 undergo division or not. This is measured by the area under the curve (AUC) in the ROC
760 diagram. The AUC can very between 0.5 (stochastic relation) and 1 (fully determined). 95%
761 Confidence intervals for AUC values were calculated using the 'ROC curve analysis' tool of
762 MedCalc software (available at https://www.medcalc.org/ index.php).
763
764 **Cellular Potts model of somite division**

765 To understand the influence of mechanical stretching on somites and the somite division
766 observed *in vivo*, we constructed a two-dimensional mathematical model based on the
767 Cellular Potts Model (Glazier & Graner, 1993; Graner & Glazier, 1992), representing a cross-
768 section through a three-dimensional somitic tissue.
769
770 We made use of a compartmentalized Cellular Potts model (CPM), also known as Glazier-
771 Graner-Hogeweg model. The model was implemented using CompuCell3D, an open source
772 modeling package based on the CPM (Swat et al., 2012). CompuCell3D's
773 'compartmentalized cell' module implements the compartmental CPM that represents
774 biological cells as a collection of sub-cellular domains, each identified by a unique cluster
775 index. This module allows specification of separate contact energies between the domains of a
776 single cell (internal parameters) as well as specification of external contact energy parameters
777 between cells of the same type and of different types. For more information on CPM
778 modeling or compartmentalized cell module, please refer to Swat *et al.* (Swat et al., 2012).
779 Briefly, the compartmentalized CPM projects biological cells on a (usually regular,
780 rectangular) lattice as domains of (usually) connected lattice sites. Each lattice site, $\vec{x}$, is
781 associated with a domain index $\sigma(\vec{x})$ that identifies a biological cell, a cellular compartment,
782 or a volume element of extracellular material. Cell identification number $\sigma = 0$ usually
783 represents a generic 'medium'. Each domain σ has a type label $\tau\left(\sigma(\vec{x})\right) \in \mathbb{N}$ to represent the
784 generic 'type' (subcellular domain, ECM, and so forth) and an additional label $\xi\left(\sigma(\vec{x})\right) \in \mathbb{N}$
785 that bundles compartments to a biological cell or connected extracellular material. Although
786 each individual object (subcellular compartment, ECM medium etc.) has its own unique
787 domain index σ, many objects may be associated with the same type label τ.
788
789 The evolution of our CPM is governed by a force-balance, represented by a Hamiltonian, *H*,

$$H = H_{contact} + H_{volume} + H_{spring} \ , \qquad (Eq.\ 1)$$

790

791 which describes the dynamics of cells (e.g. cell behaviors, properties and interactions). The
792 Hamiltonian is minimized using a Metropolis algorithm that mimics microscopic membrane
793 and material fluctuations, such that both the equilibrium and the transient towards the
794 equilibrium can be physically and biologically interpreted (Newman & Barkema, 1999).
795 $H_{contact}$ represents the cell adhesion where cell-cell and cell-medium interactions take place
796 through contact energies. The size of the interface between two cells defines the contact
797 energy and is given by:

798

$$H_{contact} = \sum_{(\vec{x},\vec{x}')} J_{\tau(\sigma(\vec{x})),\tau\left(\sigma(\vec{x}')\right)} \left(1 - \delta_{\sigma(\vec{x}),\sigma(\vec{x}')}\right) \qquad (Eq.\ 2)$$

799

800 Here, $J_{\tau(\sigma(\vec{x})),\tau\left(\sigma(\vec{x}')\right)}$ is the bonding energy between two neighboring cell types $\tau(\sigma(\vec{x})$ and
801 $\tau(\sigma(\vec{x}'))$, and $\delta_{\sigma(\vec{x}),\sigma(\vec{x}')}$ is the Kronecker delta term in which adhesion is restricted to the cell
802 membranes by eliminating the contributions from the neighboring lattice sites belonging to
803 the same cell. If $\sigma(\vec{x}) = \sigma(\vec{x}')$, the delta function returns a value of 1 and 0 otherwise. The
804 term H_{volume} in the Hamiltonian specified in Eq. 1 is given by:

805

$$H_{volume} = \sum_{\sigma} \lambda_{volume}\ (\sigma).\ [v(\sigma) - V(\sigma)]^2 \qquad (Eq.\ 3)$$

806

807 and constrains the cell volume, $v(\sigma)$, close to a resting volume $V(\sigma)$. The Lagrange multiplier
808 λ_{volume} represents cell elasticity - higher values of λ_{volume} reduce fluctuations of cell's
809 volume from its target volume.

Compartments of cells and subunits of the extracellular matrix can be mechanically coupled by connecting their centers of mass using springs. Each spring contributes an additional energy bias H_{spring} to the Hamiltonian in *Eq. S2*.

$$H_{spring} = \sum \lambda_{ij} \left(l_{ij} - L_{ij}\right)^2 \qquad (Eq. 4)$$

where l_{ij} is the absolute distance between the center of masses of cells i and j and L_{ij} is the specified target spring length. $\lambda_{ij}$is an elasticity parameter. Springs rupture if they exceed a threshold length; new springs are formed if cells move within a threshold distance. In our simulations, we have many cell types (epithelial internal compartments, extracellular matrix (ECM), and epithelial cell (apical)) which are connected using springs. Details on these cell-specific spring lengths and elasticity are explained in the next sections of the supplementary material.

The CPM is updated using a Metropolis algorithm, which mimics the extension and retraction of pseudopods of the biological cells, and fluctuations of the extracellular matrix materials. The algorithm iteratively selects a lattice site $\vec{x}$ and attempts to copy its cell index $\sigma(\vec{x})$ into a randomly chosen adjacent lattice site $\vec{x}'$. This is called a copy attempt. The probability of accepting or rejecting the attempted copy update is based on the energy minimization criteria and follows Boltzmann probability,

$$P\left(\sigma(\vec{x}) \rightarrow \vec{x}'\right) = \begin{cases} 1 & ,\Delta H\left(\sigma(\vec{x}) \rightarrow \vec{x}'\right) < 0 \\ e^{\frac{-\Delta H\left(\sigma(\vec{x}) \rightarrow \vec{x}'\right)}{T}} & ,\Delta H\left(\sigma(\vec{x}) \rightarrow \vec{x}'\right) \geq 0 \end{cases} \qquad (Eq. 5)$$

where $\Delta H(\sigma(\vec{x}) \rightarrow \vec{x}')$ represents the change in the Hamiltonian due to the copy attempt. *Eq. 5* shows that if the attempted copy update will reduce the energy, i.e. $\Delta H(\sigma(\vec{x}) \rightarrow \vec{x}') < 0$, the update is accepted with a probability of 1. However, if the energy increases due to the copy-attempt, the system follows Boltzmann probability to accept or reject a copy-attempt. The parameter T is the cellular temperature, representing the amplitude of active cell membrane fluctuations or fluctuations of the extracellular materials.

The model included the following assumptions: (i) the tissue surrounding the somite can be approximated as elastic, and was modeled as a non-specified extracellular matrix (ECM); (ii) the somite consists of polarized epithelial cells forming the outer layer (Dias et al., 2014), while the somite core (somitocoel) consists of unpolarized mesenchymal cells. The mesenchymal cells in the core of the somite were represented by single-compartment, non-coupled and non-polarized cells. Following Dias *et al.* (Dias et al., 2014) the epithelial cells in our model consisted of three domains, called 'apical', and 'lateral' and 'basal' (Fig S9). The three compartments were initially distributed at random inside an epithelial cell and after a brief relaxation period of 1500 MCS (epithelial polarization time), these compartments were connected internally to one another using linear elastic springs (Eq. 4). To achieve epithelial elongation (Fig S9), target lengths of all internal springs ($L_{apical-lateral}$, $L_{apical-basal}$, $L_{lateral-basal}$) were individually incremented by 1 every 20th MCS within the elongation time frame (1500 MCS), until every spring reached its final specified target length ($L_{apical-lateral} = 15, L_{apical-basal} = 30, L_{lateral-basal} = 20$). The ECM, with its main functional component fibronectin *in vivo* ("P.Rifes, thesis: Fibronectin cues during somite formation, Universidade de Lisboa (2013)," n.d.), was modeled as a network of cells. These ECM cells were also connected to each other using elastic springs of target length

855 $L_{ecm-ecm} = 10$ with elastic stiffness $\lambda_{ecm-ecm} = 200$. This was necessary to obtain a
856 desired stiffness of the ECM in order to keep it intact during and after stretching.
857
858 We first attempted to construct a well-organized, initial epithelial structure as a starting point
859 for the stretching model. Contact energies between domains as well as contact energies with
860 other cell types and the ECM were set according to S3 Table. In absence of quantitative
861 values for the adhesion strengths and interfacial tensions between the cells, we estimated
862 parameter values for which a stable epithelial monolayer is maintained in our simulations,
863 followed by parameter sensitivity studies. We assumed the apical domains of adjacent
864 epithelial cohered strongly, following Dias *et al.*'s (Dias et al., 2014) assumption mimicking
865 the distribution of N-Cadherin *in vivo* (Chal, Guillot, & Pourquié, 2016). The lateral domains
866 of epithelial cells (between the apical and basal domains) adhere strongly to each other,
867 similar to Cadherin mediated cohesion *in vivo* (Horikawa et al., 1999; Kimura et al., 1995).
868 To represent the apical actin ring, each center of mass of an apical unit was connected to the
869 center of mass of neighboring apical domains on either side (left and right) using elastic
870 springs of a resting length of $L_{ij} = 4$ with elastic stiffness $\lambda_{apical-apical} = 100$.
871
872 The monolayer of epithelial cells was constructed by initializing the simulation with a
873 collection of mesenchymal cells surrounded by an elastic ECM. We selected a mesenchymal
874 cell at the boundary with the surrounding ECM and made it epithelial. This first epithelialized
875 cell induced MET in neighboring cells based on basolateral contact (Baum & Georgiou, 2011;
876 Campbell et al., n.d.), which finally led to a fully epithelialized somite-like structure (initial
877 phase of Movie S3).
878

879 After a stable, somite-like, epithelial structure had formed, we gradually strained the
880 extracellular matrix in our simulations, in order to mimic the experimental setup. To this end,
881 we connected two 'walls' constructed out of immobile cells to the left and right-hand ends of
882 the ECM using stiff elastic springs and slowly moved the walls apart by 1 pixel every 50
883 MCS, using a technique introduced previously for simulating the compression of tissue
884 spheroids (Marmottant et al., 2009) and the application of stents in arteries (Tahir, Niculescu,
885 Bona-Casas, Merks, & Hoekstra, 2015)
886
887 The stretching rate was sufficiently slow (walls moved outward by 1 pixel every 50 MCS),
888 such that it did not damage the ECM cells (Phase 2 in Movie S3). We tested three MET
889 scenarios for their ability to allow the stretched somite to divide into epithelialized daughter
890 somites. We first assumed that somites can divide by reorganization of existing epithelial cells
891 and allowed no MET after the stretching. We could successfully deform the somite by
892 stretching, but neither small nor large strains induced somite division (Fig S10, top row). This
893 suggested the necessity of an MET mechanism to enable somite division. In the second
894 scenario, a mesenchymal cell underwent MET after contact with the surrounding ECM for a
895 certain time (600 MCS). We did not observe somite division for different levels of
896 deformation, probably because intercellular connections between epithelial cells did not
897 soften completely upon stretching, thereby avoiding sufficient contact between mesenchymal
898 somitocoel cells and the surrounding ECM to induce additional MET (Fig S10, middle row).
899 In the third scenario, the MET occurred after sufficiently long contact of mesenchymal cells
900 to the basal or lateral membrane of epithelial cells (600 MCS). Upon stretching, several
901 springs between neighboring apical compartments released and mesenchymal cells from the
902 core became exposed to the lateral or basal membranes of epithelial cells leading to additional
903 MET. These additional epithelial cells disturbed the equilibrium and could not get

incorporated into the original epithelial ring. So, the epithelium started to reorganize and divide into daughter somites (Fig S10, bottom row and Phase 3 in Movie S3).

Based on our observations that daughter somites are separated and presumably stabilized by a newly forming fibronectin matrix (Fig S4), we also implemented a similar rule for ECM production by the basal units of epithelial cells. If the basal domain of an epithelial cells is not attached to a specified amount of ECM (given by threshold value) for a certain duration, it produces an additional ECM cell. This production continues until the threshold value is reached again. Such production of the fibronectin allows the dividing somites to separate from each other permanently. The parameters used in the simulations are shown in the S3 Table. For a systematical analysis of how well the geometry of stretched somite predicts division we applied lateral wall displacements of 30 to 110 pixels (15 to 55 pixels per side), resulting into aspect ratio values similar to stretched somites *in vivo* (Fig 3G).

The *in silico* somite model can be parameterized to the experimentally observed ratio of mesenchymal and epithelial cells**.** Fig S11 shows that, following the MET based on the basolateral contact rule, initial epithelialization of the somite and division of the somites after stretching can be achieved with a large core and small core somite.

In order to further validate the *in silico* model, we also tested the influence of decreased cohesion between lateral domains of epithelial cells in epithelializing, non-stretched somites. Similar to results in *N-Cadherin/cad11* double-homozygous mouse mutants (Horikawa et al., 1999), we observed subdivisions into small cell clusters of epithelioid morphology (Fig S12).

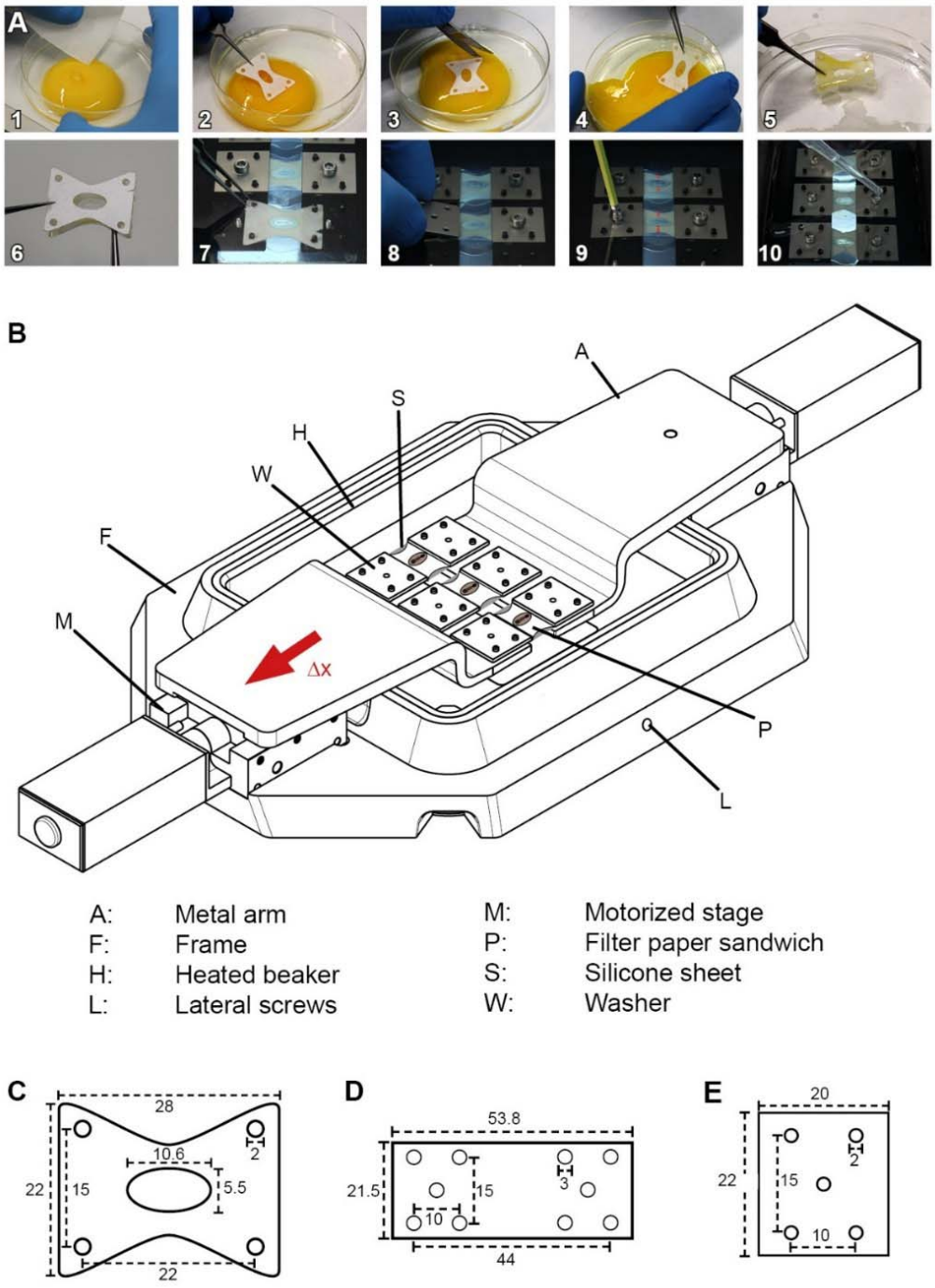

Fig S1: Chick embryo stretching *ex ovo*, experimental setup. (A) Explantation procedure (Schmitz et al., 2016). (1) An egg is cracked into petri-dish and thick albumen removed from top of the yolk. (2) A filter paper carrier is placed on top of the yolk, surrounding the blastoderm. (3) The filter paper carrier is cut loose from the surrounding vitelline membrane and (4) removed from top of the yolk. (5) Remaining yolk is carefully washed away in a

saline bath. (6) The embryo is sandwiched with a second filter paper carrier. (7) The filter paper sandwich is submerged into the medium and hooked into the pins of the motorized arms. A thin sheet of PDMS protects the embryo from convection of the medium. (8) Washer plates clamp the filter paper sandwich to the metal arms and (9) are carefully pressed down by nuts. Filter paper sandwiches are cut along dashed red lines for later stretching of embryos. (10) The medium is covered with a layer of light mineral oil. (B) Schematic view of the embryo stretcher. The frame carries the motorized stages and keeps the temperature-controlled medium container in position. The whole setup is placed on a motorized x-y-stage, embryos are imaged from above and illuminated from below through the glass bottom of the medium container. (C) Filter paper carrier dimensions (in mm). (D) Dimensions of stencil for PDMS sheets (in mm). (E) Dimensions of metal washers used to clamp the filter paper (in mm).

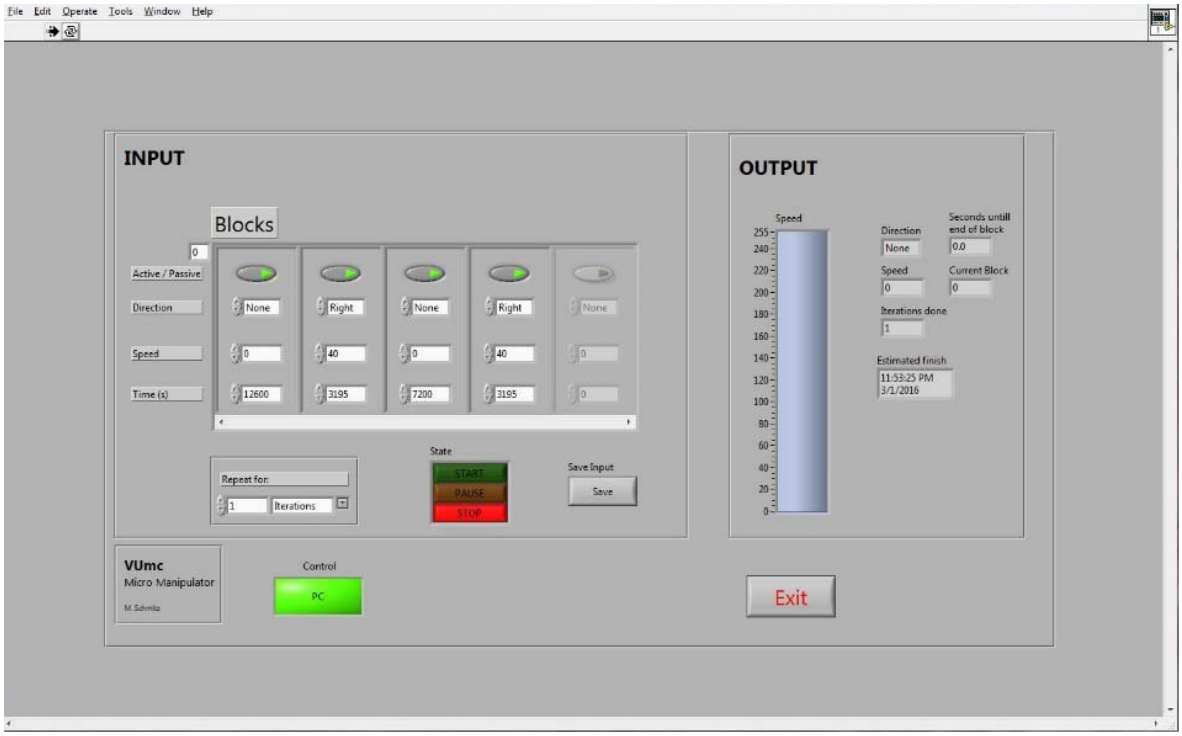

945

946 **Fig S2: User interface of the custom-made LabVIEW routine used to control one**
947 **motorized translation stage of the embryo stretcher.** Four experimental blocks are
948 activated, defining the resting time after covering the culture medium with light mineral oil
949 (12600 s/3.5 hrs), the first pulling block (3195 s), a resting time in between pulls (7200 s/2
950 hrs) and the second pulling block (3195 s).

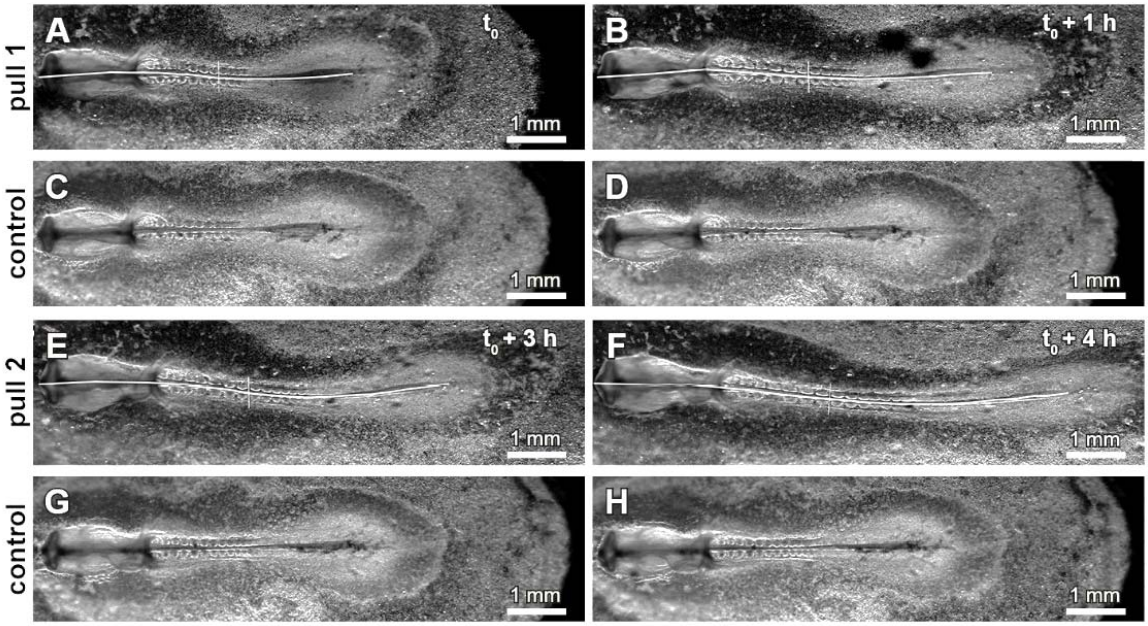

Fig S3: Macroscopic deformation of pulled embryos. Before application of the first pull, experimental embryo (A) and control (C) are similar in axial length. The first pull increases the axial length of the pulled embryo considerably compared to the control (compare B and D). This length difference remains over the waiting period between first and second pull (compare B and D and E and G). The second pull increases the length difference between pulled embryo and control even further (compare F and H).

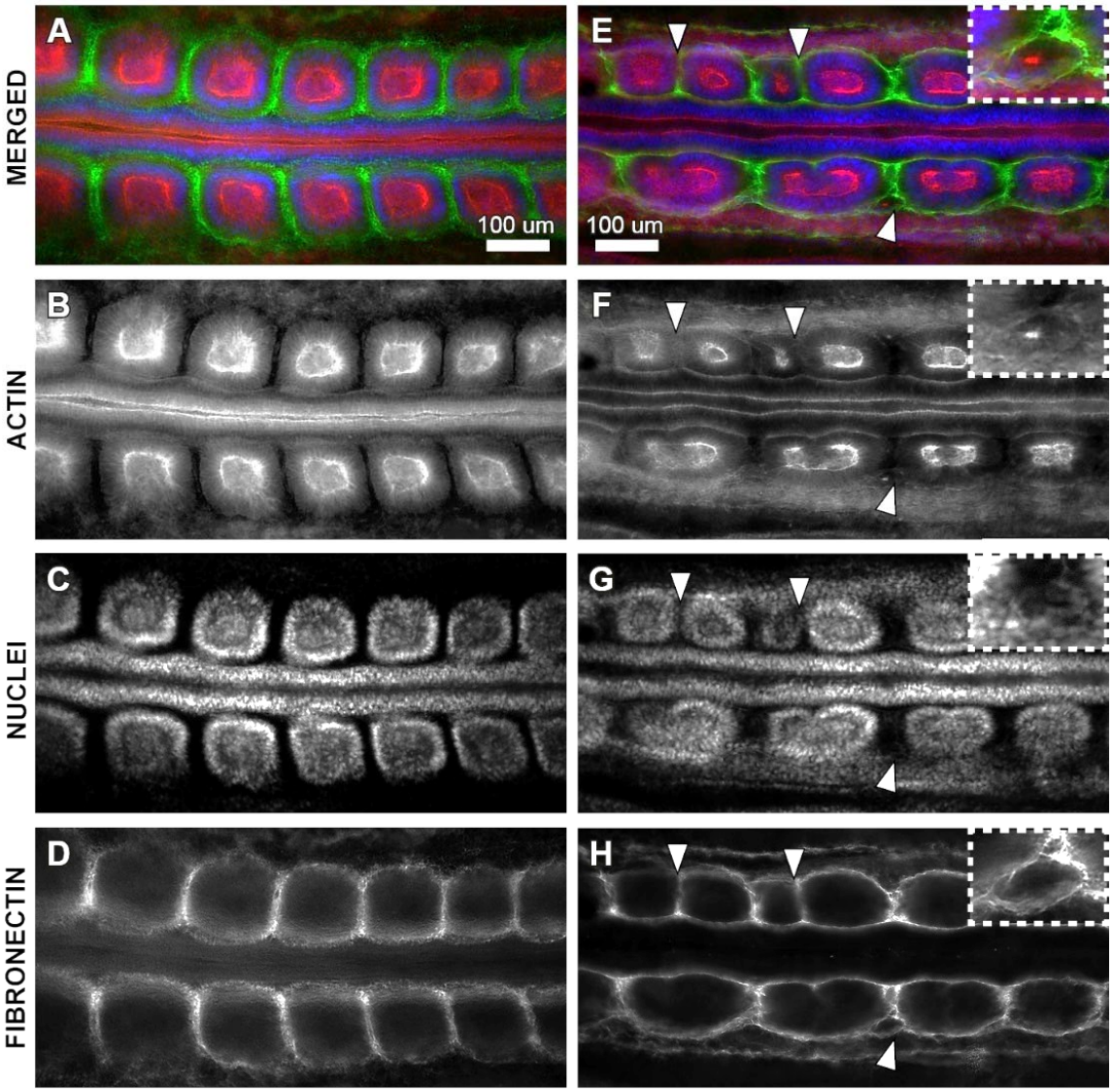

Fig S4: Fibronectin distribution around daughter somites. Widefield fluorescent micrographs of control embryo (A-D) and stretched embryo (E-H) stained for actin (red), DNA in cell nuclei (blue) and extracellular matrix component fibronectin (green). Ventral view, anterior is to the left. Daughter somites are surrounded and separated from each other by a newly formed fibronectin matrix (white arrowheads in E and H) and can be extremely small (inset E to H) and lacking a mesenchymal core.

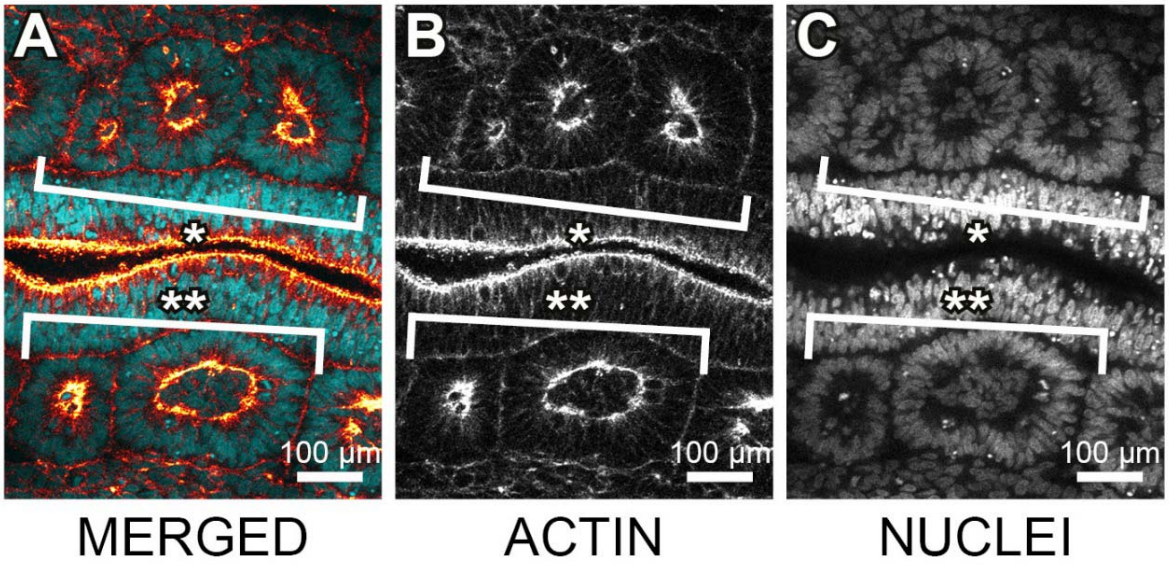

Fig S5: Versatile daughter somite morphologies. Confocal micrograph of daughter somites on both sides of the midline in stretched and fixated chick embryo stained for actin (red) and DNA in cell nuclei (blue). Anterior is to the left, ventral view. Daughter somites do not only result from splitting into anterior and posterior compartment of original somite, but can also reorganize into three daughter somites (*) or two unequally sized daughter somites (**).

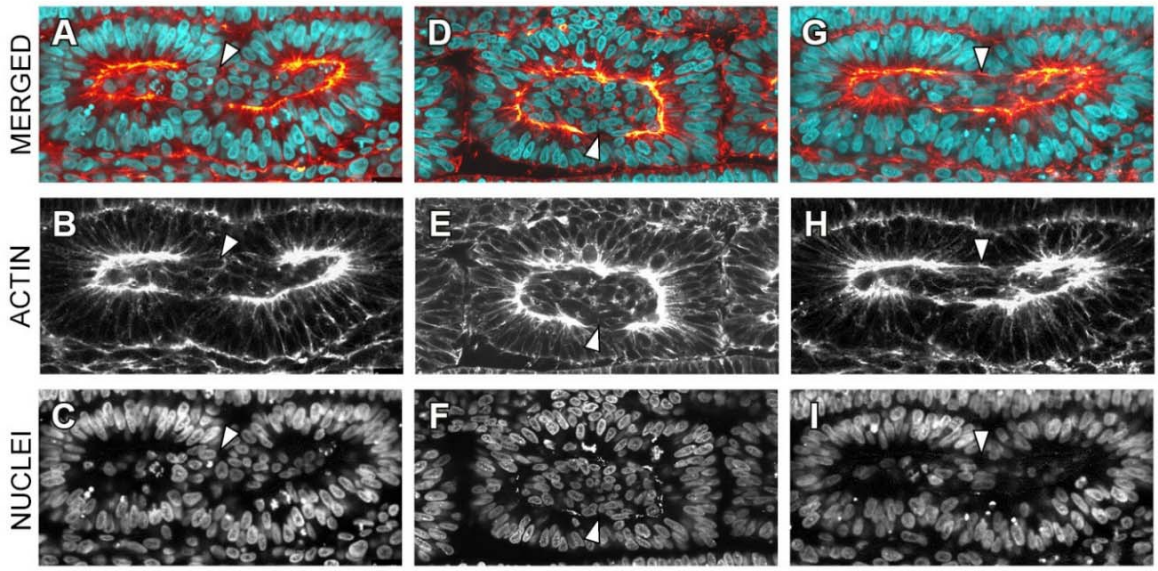

Fig S6: Fracture of epithelial sheet and potential MET of mesenchymal somitocoel cells. Confocal micrograph of somites, fixated during daughter somite formation in stretched chick embryos, stained for actin (orange) and DNA in cell nuclei (cyan). Anterior is to the left. White arrowheads indicate discontinuities in the apical actin ring of the somitic epithelium, suggesting a local opening of the epithelial sheet and potential interfaces for the recruitment of additional mesenchymal cells from the somitocoel for their incorporation into the existing epithelium.

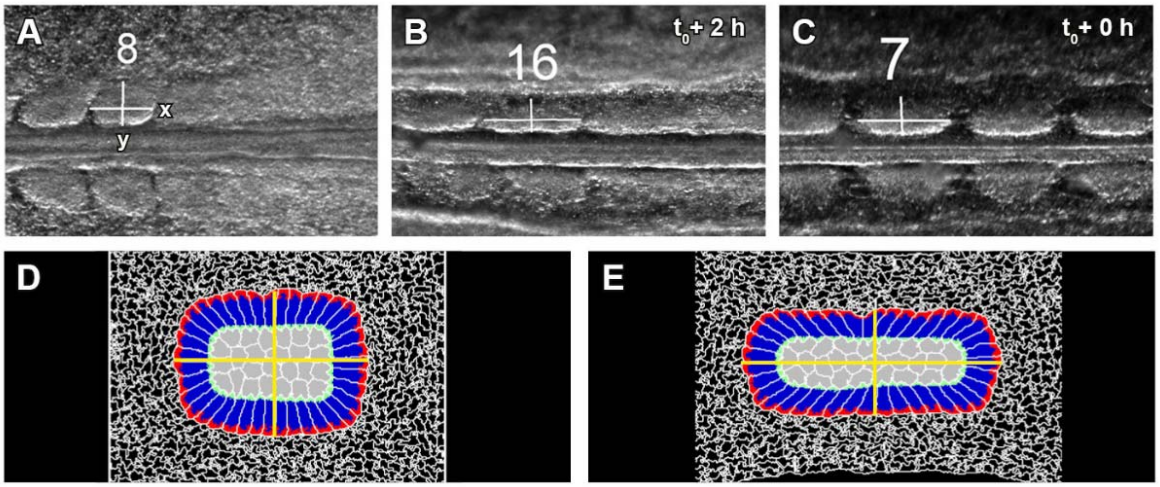

Fig S7: Determination of somite aspect ratios. Measuring the length (x) and width (y) of somites upon separation from the anterior tip of the PSM in control embryos (A) and stretched embryos (B), and after application of the second pull (C). Somites in (B) and (C) underwent division later. Anterior is to the left. Aspect ratio determination *in silico* before (D) and after (E) the pull.

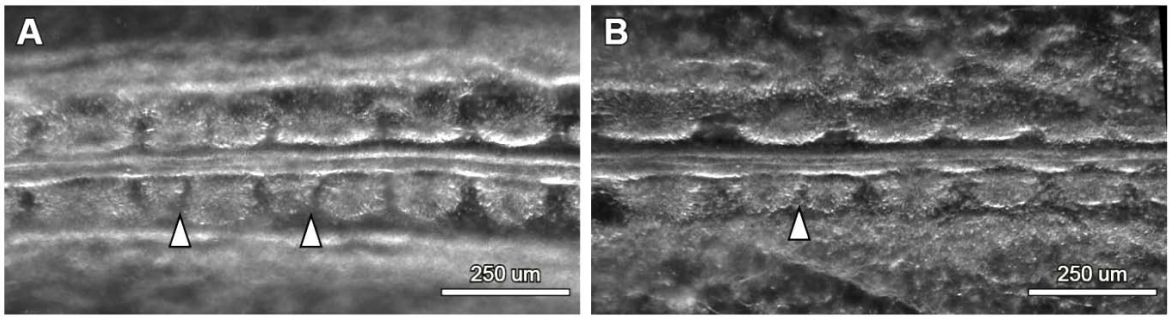

Fig S8: Unequally sized daughter somites. Anterior is to the left. White arrowheads indicate gaps between unequal daughter somite pairs.

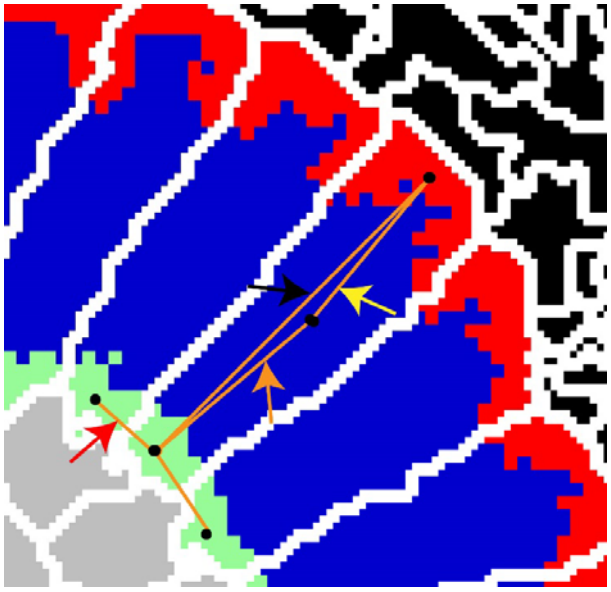

Fig S9: Snapshot of various cell types present in the simulations**.** Mesenchymal cells shown in grey. Epithelial cells consist of three domains: Apical (green), lateral (blue) and basal (red) domain. Center of masses (black dots) of epithelial cell domains are connected internally to each other using elastic springs. The springs between apical and lateral domain (orange arrow), lateral and basal domain (yellow arrow) and apical and basal domain (black arrow) are indicated. Each epithelial cell has the same spring configuration helping epithelial cells to elongate after polarization. Apical domains of neighboring are also connected via springs (red arrow) to trigger the formation of single layer of epithelial cells. Black cells in the upper right-hand corner represent ECM.

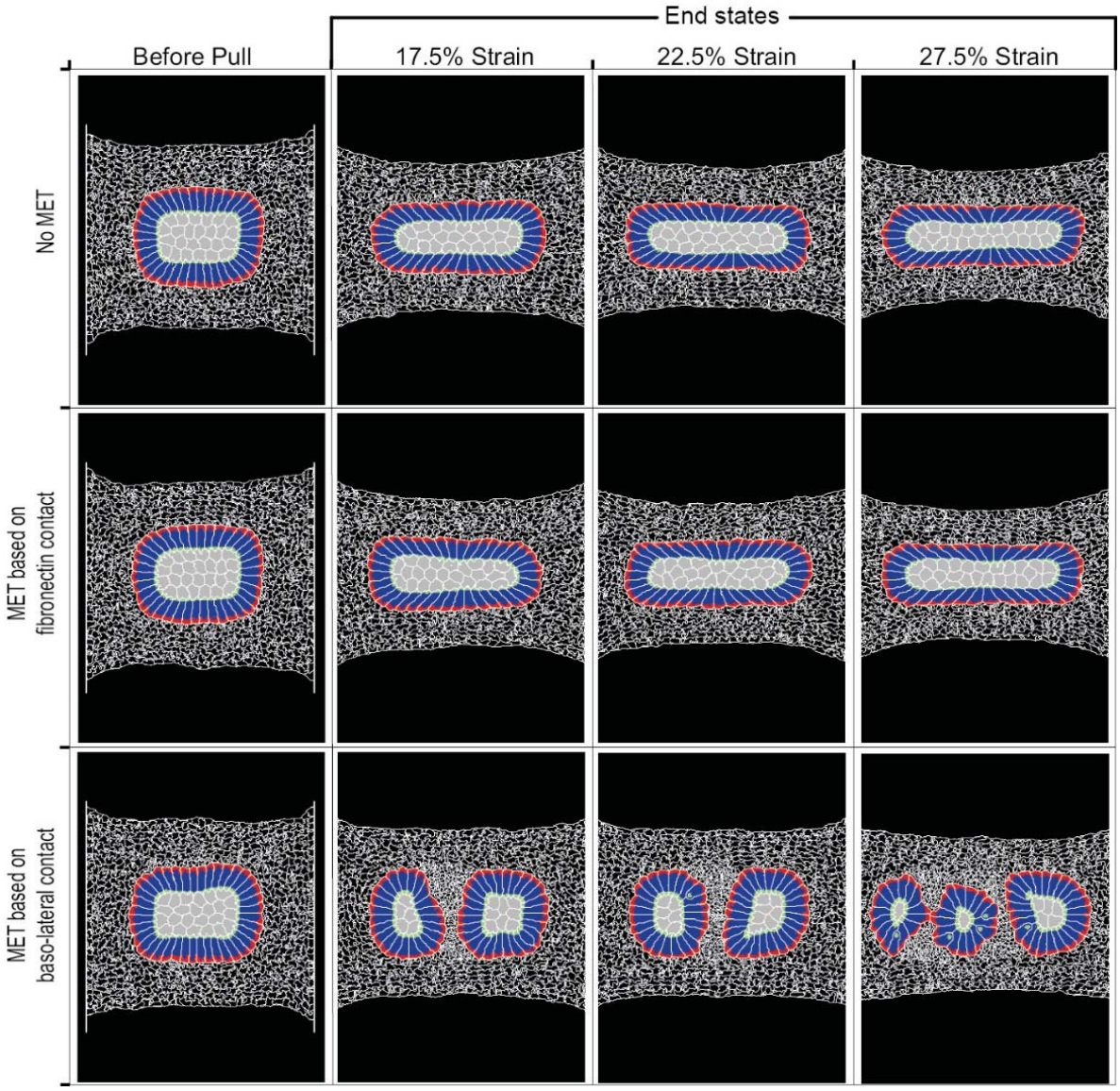

Fig S10: End states of simulations, testing different mesenchymal-epithelialization transition rules. Fully epithelialized somites were exposed to different strains (strain given by relative change in distance between movable walls), inducing aspect ratios of 2.5 (17.5% strain), 2.9 (22.5% strain) and 3.3 (27.5%) (compare Fig 3G). *Top row*: No MET was allowed after the pull. This was due to our initial hypothesis that somite doubling is nothing more than the reorganization of existing epithelial cells. We applied different strain values to see if high strain might lead to somite doubling. No somite division was observed. *Middle row*: MET was allowed after the pull if a cell had been in contact to the surrounding ECM matrix for a

certain period of time. This MET rule did not allow somite division under various strain conditions. *Bottom row*: A new rule allows MET of mesenchymal cells upon contact to the lateral or basal membranes of epithelial cells. Formation of stable daughter somites could be observed. Both, ECM (fibronectin) induced epithelialization and basolateral contact induced epithelializing were sufficient to generate fully epithelialized somite-like structures prior to stretching.

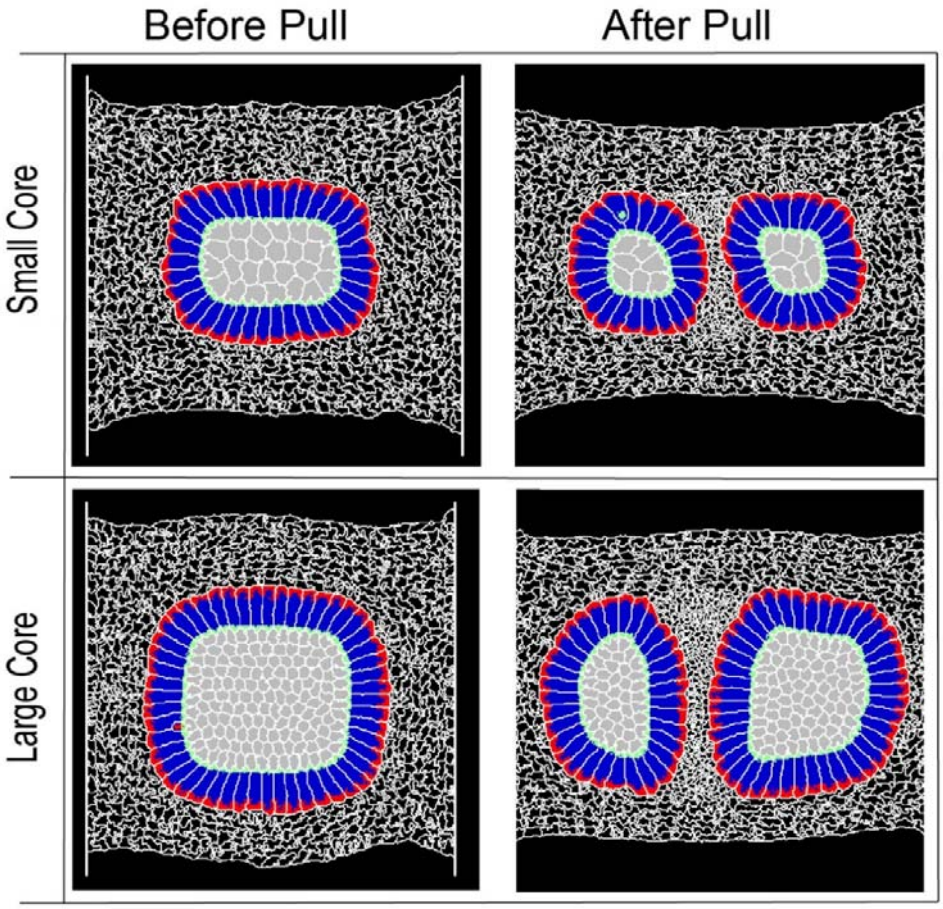

Fig S11: Different somite core sizes and mesenchymal cell sizes. *Top row:* Small core somite before and after pull showing somite divisions after pull. Similar response of somite division can also be seen in the large core somite (*Bottom row*). This in silico model of somite division also allows to change the size of the cells. This is evident by comparing the size of the core mesenchymal cells (in grey) in the top and bottom rows.

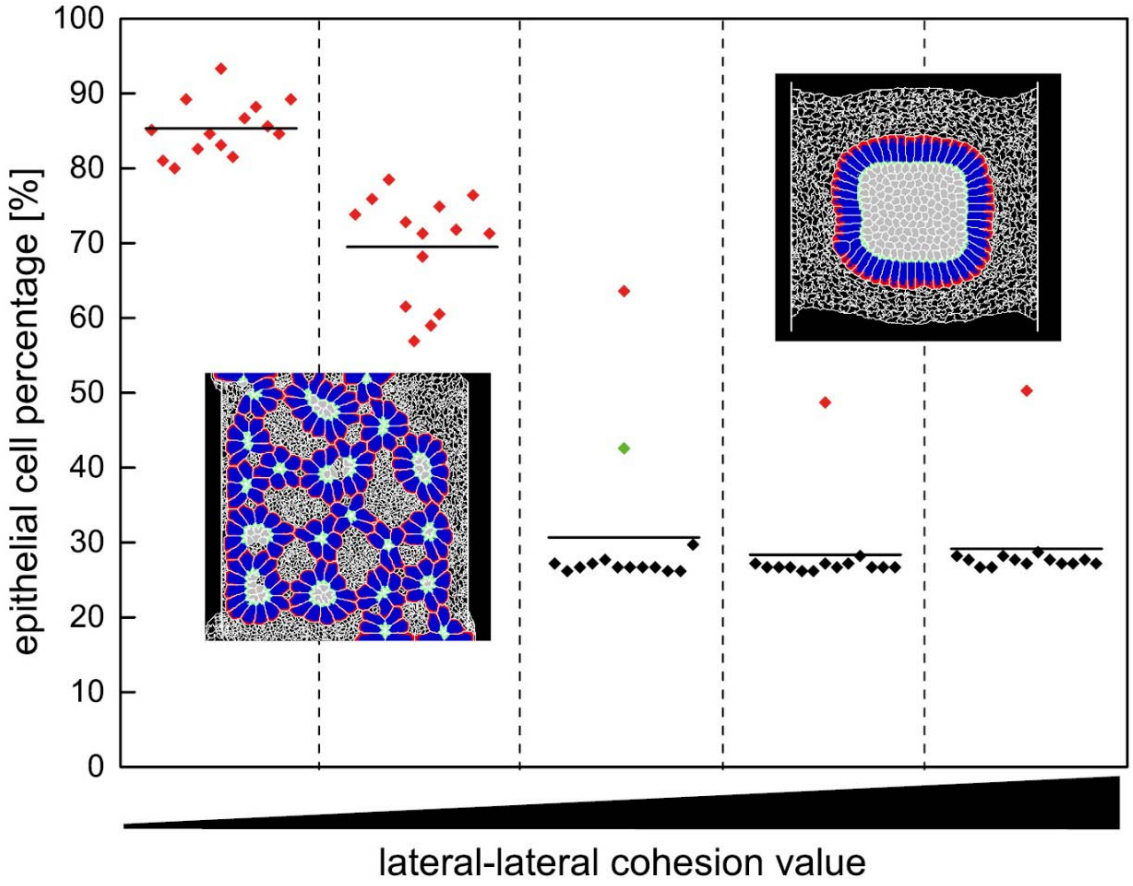

Fig S12: Influence of cohesion between lateral domains of epithelial cells on daughter somite number and epithelial cell percentages *in silico*. Cohesion between lateral domains of epithelial cells was varied in non-stretched somites to study the effect on somite formation. With low cohesion, almost 85% of mesenchymal cells became epithelial. This increase in epithelial cell number resulted in the formation of many epithelialized cell clusters (red data points), whereas for high cohesion values, we observed no somite division except for one case (green data point). Non-dividing somites are indicated by black data points.

S1 Table: Mechanical strain caused by application of the external mechanical pull.

Daughter somite formation?	Embryo No.	Distance per pull [mm]	Mechanical Strain [%]	
			pull 1	pull 2
Yes	1	3.85	21	19
	2	3.8	21	20
	3	3.7	21	20
	4	3.85	26	16
	5	3.85	26	21
	6	3.85	21	17
	7	3.85	26	15
	8	3.85	25	17
	9	3.85	26	15
	10	3.9	27	24
	11	3.95	28	19
	12	3.95	18	20
	13	3.95	24	22
	14	3.95	22	18
	15	3.95	20	19
	16	3.95	22	15
No	17	3.85	23	19
	18	3.8	22	18
	19	3.85	21	19
	20	3.85	25	13
	21	3.7	18	17

S2 Table: Somite formation rates for stretched embryos, with and without daughter somite formation, and control embryos.

Daughter somite formation?	Embryo No.	Somite No. initial	Somite No. final	Time interval [min]	Somite formation rate [min/somite]
YES	1	10	18	610	76.3
	2	9	19	785	78.5
	3	14	22	636	79.5
	4	14	20	498	83.0
	5	13	20	618	88.3
	6	14	21	536	76.6
	7	14	20	520	86.7
	8	12	19	524	74.9
	9	13	21	584	73.0
	10	6	13	565	80.7
	11	12	17	451	90.2
	12	17	24	556	79.4
	13	15	24	723	80.3
	14	15	21	510	85.0
	15	15	22	553	79
	16	17	25	523	65.4
				Average ± Stdev.:	**79.8 ± 6.2**
NO	17	15	22	578	82.6
	18	11	21	795	79.5
	19	17	23	413	82.6
	20	15	21	510	85
	21	12	22	826	82.6
				Average ± Stdev.:	**82.5 ± 2.0**
Controls	22	6	12	527	87.8
	23	6	23	1301	76.5
	24	7	20	915	70.4
	25	8	21	1079	83
				Average ± Stdev.:	**79.4 ± 7.6**

1034 **S3 Table: Parameters values used in the Cellular Potts Model.**

Parameter	Value
Simulation lattice size	400 pixels x 300 pixels
Simulation temperature (Noise)	100
Total simulation steps	130000 Monte Carlo steps (MCS)
Moment pull	60000 MCS
Pull duration	10000 MCS
Epithelial target volume V_{epi}	300 pixel (9% Apical, 70% Lateral and 21% Basal)
Epithelial volume stiffness $\lambda_{volume-epi}$	100
Mesenchymal volume V_{mes}	195 pixels
ECM volume stiffness $\lambda_{volume-mes}$	30
ECM cell volume V_{ecm}	75 pixels
ECM volume stiffness $\lambda_{volume-ecm}$	25
Epithelial polarization time	1500 MCS
Epithelial elongation time	1500 MCS
Epithelial sub-cellular units spring stiffness	500
Apical – Lateral spring length	15 pixels (absolute distance between center of masses of two cells)
Apical – Basal spring length	30 pixels (absolute distance between center of masses of two cells)
Lateral – Basal spring length	20 pixels (absolute distance between center of masses of two cells)
Apical – Apical spring stiffness	100
Apical – Apical spring length	4 pixels (absolute distance between center of masses of two cells)
ECM - ECM spring stiffness	200
ECM – ECM spring length	10 pixels (absolute distance between center of masses of two cells)
Contact Energies	
Inter-cellular (external) adhesion energies	
$J_{med-apical}$, $J_{med-lateral}$, $J_{med-basal}$, $J_{med-mes}$, $J_{med-ecm}$,	300, 300, 300, 300, 30
$J_{apical-apical}$, $J_{apical-lateral}$, $J_{apical-basal}$, $J_{apical-mes}$, $J_{apical-ecm}$	3, 150, 150, 10, 160
$J_{lateral-lateral}$, $J_{lateral-basal}$, $J_{lateral-mes}$, $J_{lateral-ecm}$,	70, 100, 200, 130
$J_{basal-basal}$, $J_{basal-mes}$, $J_{basal-ecm}$	30, 280, 40
Internal adhesion energies (between domains)	
$J_{apical-lateral}$, $J_{apical-basal}$, $J_{lateral-basal}$	2, 20, 2

Movie S1: Control embryo

Time-lapse movie of the development of a control chick embryo (stage HH9+), cultured ex ovo, mounted in submerged filter paper sandwiches in the stretch setup for 19 hours, without stretching. Timer is in hours.

Movie S2: Stretched embryo showing somite divisions

Time-lapse movie of the development of an experimental chick embryo (stage HH10), cultured ex ovo, mounted in submerged filter paper sandwiches in the stretch setup for 17,5 hours, and stretched at a speed of 1.2 µm/s along the anterior-posterior (AP) axis, in two pulls. First the overview is shown, afterwards a zoom in at the mesoderm. The stretching deforms the embryos slowly but substantially, while development progresses without damage. During the deformation, somites divide into daughter somites of different sizes, as marked by the white arrowheads in the zoom. For example: the first arrowhead shows an asymmetric somite division (lower left), while the second arrowhead shows a symmetric division (upper left).

Movie S3: Somite epithelialization and division *in silico*

Simulation video of dividing *in silico* somites, consisting out of frames of every 500th Monte Carlo Step. We tested different rules in our Cellular Potts model concerning cellular behavior in the deformed somites, to find out the most likely mechanism for the somite division to take place. Daughter somite formation in stretched somites could only successfully be induced when a MET of mesenchymal core cells upon contact to the basal or lateral membranes of epithelial cells was allowed.